QUANTITATIVE CHARACTERIZATION OF THERMOPHYSICAL PROPERTIES IN COMPUTATIONAL HEAT TRANSFER

Kaushik A. Iyer
B. Tech., Indian Institute of Technology
Madras, India, 1991

A thesis submitted to the faculty of the
Oregon Graduate Institute of Science and Technology
in partial fulfillment of the
requirements for the degree
Master of Science
in
Materials Science and Engineering
July, 1993

The thesis "Quantitative Characterization of Thermophysical Properties in Computational Heat Transfer" by Kaushik A. Iyer has been examined and approved by the following Examination Committee:

LEMMY L. MEEKISHO
Assistant Professor
Thesis Advisor

DAVID G. ATTERIDGE
Associate Professor

JACK H. DEVLETIAN
Professor

ACKNOWLEDGEMENTS

First, I would like to express my gratitude to my thesis advisor, Dr. Lemmy Meekisho, for his guidance, cooperation and patience. His view of what a student-advisor relationship should be enabled the pursuit of research excellence in the highest scientific traditions. I would also like to thank Drs. David Atteridge and Jack Devletian for their constructive input in getting my thesis in order. Lastly, my eternal gratitude to my family, whose continuing amazement at the achievements of my humble intellect drive me to pursue yet another degree.

TABLE OF CONTENTS

LIST OF FIGURES

ABSTRACT

Quantitative Characterization of Thermophysical Properties
in Computational Heat Transfer

Kaushik A. Iyer, MS
Supervising Professor : Lemmy Meekisho

The most fundamental step in the development of a predictive model for microstructure and residual stress distribution in steels is the accurate representation of the transient temperature field. Three constituents of a database of thermophysical properties, namely the thermal conductivity, volumetric specific heat capacity and convective heat transfer coefficient, were isolated and their effects quantified on the accuracy of temperature field predictions using finite element analysis (FEA). The most critical parameter in the heat transfer process was ultimately identified to be the temperature dependent convective heat transfer coefficient. It was determined using an inverse heat transfer method, which was successfully applied to accurately establish the thermal boundary conditions for an arbitrary 3D steel geometry. The temperature dependency of the volumetric specific heat capacity in the transformation range of temperatures has to be known a priori, for which a reliable model describing alloy dependent reaction kinetics has to be developed first. Thermal conductivity and its dependency on temperature has secondary effects on the accuracy of FEA predictions. The impact of the outcome of this study lies in its relevance to the heat treatment industry.

CHAPTER 1

INTRODUCTION

Heat treatment of low alloy steels is an economical way to produce components with reliable service properties. The steel chemistry and the kind of heat treatment contribute to the determination of material properties. The broad objectives of controlling the heat treatment process include microstructural control to enhance properties such as wear resistance and toughness, achievement of a predetermined hardness distribution, minimizing residual stresses and reducing distortion.

In order that these goals are met, the synergistic effects of temperature, microstructure and stress have to be well understood.

The guiding philosophy behind the current work is the development of a coupled finite element methodology for the calculation of the temperature field, microstructural evolution and mechanical response i.e; residual stresses and distortion, for an arbitrarily shaped 3D steel geometry with a chemistry typical of structural steels. However, the immediate objective is to establish how critical the representation of the temperature dependency of thermophysical properties is, as input data, in the development of a general predictive model applicable to a variety of steels and geometries.

Early work in this area was done by Henwood [1], who developed an analytical model for computing weld microstructures based on theoretical models found in the literature. Microstructural changes in the weld fusion and heat-affected zones were tracked as the material progressed through a thermal cycle. Austenite grain size was determined using the Ashby grain growth relationship [2] while austenite decomposition

was modeled using Kirkaldy decomposition kinetics [3]. The transient heat flow was modeled in two dimensions. A finite element program which provided an approximate solution to the 3D transient heat flow problem described by the quasi-harmonic equation, was presented in [4]. Goldak et al [5] made transient temperature field computations and modeled moving heat sources, nonlinear thermal properties and heats of fusion and transformation in simulating a welding process, using a finite element formulation for 3D transient heat flow. The primary database of non-linear thermophysical properties used in this study was obtained from Goldak's work [5].

Present day finite element codes attempt to incorporate thermodynamics based prediction of the multicomponent phase diagram corresponding to a specific steel chemistry with a 3D transient heat transfer analysis. These features, when combined, can be used to perform finite element calculations of the transient temperature field taking into account microstructural effects such as latent heat, microstructural evolution during quenching. Further, calculation of the stress/strain response accounting for dilatation, transformation plasticity and creep, and, prediction of hardness distribution as a function of microstructure and cooling conditions are also possible.

Inoue, Ju and Arimoto [6] developed the finite element code "HEARTS" for the 3D simulation of various heat treatment processes such as quenching and tempering. They coupled the effects of differing cooling rates in a body on the resulting phase transformations, with the thermal stress distribution. The effect of transformation plasticity on the predicted cooling rates was also shown to be a significant factor.

Bodin and Segerberg [7] developed a procedure for the evaluation of the correctness of commercial computer model solutions for heat treatment of steel components on the basis of test heat treatments carried out on test pieces of various sizes and differing steel chemistries. Not only did they find that the programs produced results which sometimes differed considerably from each other and from the experimental results, but also that the model for phase tranformation prediction crucially affected the modeling of the quenching process. This suggests that among other factors, such as the

quality and size of the database of thermophysical properties, crucially affects the performance of a computer simulation. Simulated results are usually compared with test results to establish credibility. This being the case, the initial and process data have to be determined as carefully as possible. These comprise data relating to the material, boundary conditions relating to the process and the shape and size of the component.

A key parameter used in the calculation of the transient thermal history using finite element analysis is the heat transfer coefficient between the surface of the component and the quenchant. This parameter is a function of temperature and the geometry of the specimen. The accurate modeling of the 3D heat transfer process at the surface requires a dependable database of these film coefficient values for the specific component geometry. This can be achieved using the inverse heat transfer analysis if the geometry specific experimental values are not known, which is generally the case. The estimation of boundary conditions at the surface of a body, that caused a known temperature history at one or more interior locations, is an inverse problem. The determination of the temperature dependency of the heat transfer coefficient for air using the inverse heat transfer method is described in detail in chapter 3.

B.Hernandez-Morales et al [8] determined heat transfer coefficients using inverse techniques by quenching stainless steel and mild steel disks instrumented with thermocouples in brine, water, oil and air, under controlled conditions that ensured one-dimensional heat transfer. Their results were reproducible to within 18% and they found that the sequential function specification method produced more reasonable results than sequential matching techniques for small time increments.

Beck and Osman are major contributors to the theory of inverse methods with specific reference to the heat conduction problem. In their latest effort [9], they have used a sequential function specification method with the possibility of varying the number of future time steps used, to estimate the temperature dependent heat transfer coefficient and heat flux during a quenching process. They found the function specification method with variable number of future time steps can provide a quick and accurate analysis of

quenching of flat plates, cylinders and spherical composite bodies.

Segerberg and Bodin [10] measured and calculated the heat transfer coefficient of the curved surface of Inconel 600 cylinders with different diameters and found that the heat transfer coefficients calculated at positions halfway along the longer surface did not differ greatly for cylinders of different sizes. However, the peak values of the heat transfer coefficient differed considerably depending on the position of the interior location from which thermocouple data was used for calculation.

Once again, the goal of this work was not the prediction of microstructures, residual stresses etc. but rather an investigation of certain specific factors that eventually affect the accuracy of such predictions. More specifically, this work involved an attempt to methodically evaluate the relative importance of some of the parameters that constitute the database of thermo-physical properties and the effects of a complex, application oriented geometry, on the accuracy of a predictive model. A quarter symmetry model of the specimen is shown in figure 1.

The specific physical properties under investigation were the volumetric specific heat, the thermal conductivity and the heat transfer coefficient. The isolated and combined effects of these and of the complexity of the geometry on the 3D finite element heat transfer analysis, are discussed in Chapter 2.

The heat transfer coefficient being a strong function of geometry, it was necessary to attempt an estimation of this parameter for the specific geometry under consideration. A finite element based evaluation of this nature i.e; involving an arbitrary 3D geometry using inverse techniques, was done for the first time. The methodology and results of this study are discussed in Chapter 3.

The final chapter, Chapter 4, discusses the combined impact of the various parameters taking into account all results.

CHAPTER 2

DATABASE EXAMINATION

2.1 OVERVIEW

The first step in addressing the residual stress and/or microstructural prediction problem is the accurate description of the temperature field as a function of geometry and time under the influence of given boundary conditions. Once this transient thermal history of a steel geometry is established, it is possible to advance into the realms of microstructural development and residual stress measurement. This chapter describes some of the parameters that crucially affect the prediction of the transient temperature field using 3D finite element analysis (FEA) and their impact on the simulations.

Water quenching and air cooling of a steel specimen, whose quarter symmetry model is shown in figure 1, were studied experimentally and numerically. As mentioned earlier, the geometry of the specimen analyzed was chosen so as to represent typical parts found in real life steel manufacturing. Thermocouple data was recorded on and inside the specimen via a data acquisition system, following which, the 3D FEA was carried out. The two sets of results for the different locations were compared to determine the effects of geometry and the quality of the database of the thermophysical properties on the simulated results.

2.2 EXPERIMENTAL SETUP AND PROCEDURE

The specimen under consideration was instrumented with Type K (Chromel-Alumel) thermocouples for each experimental run. Static air cooling and water quenching processing of the specimen were conducted. For each case, two sets of specimens, each with thermocouples located at different depths from the surface were used, as shown in figures 2 and 3. One set had thermocouples positioned at 1) the center of the cavity, 2) 1" below the surface of the cavity and along the axis of symmetry, 3) 3" below the surface of the cavity and along the axis of symmetry and 4) 5" below the surface of the cavity and along the axis of symmetry. These were classified as specimen type A, shown in figure 2. The second set had thermocouples positioned along the axis of symmetry at distances or 2", 4" and 6" below the surface of the cavity section and a fourth thermocouple at the center of the bottom surface of the specimen i.e; the tip. These were classified as specimen type B, shown in figure 3.

Holes with diameters closely matching those of the thermocouple wire were drilled from the surface to the appropriate depths and the thermocouples were implanted using a spot welding technique. The portion of the thermocouple wire embedded in the metal was insulated by a Nextel ceramic braid, capable of withstanding temperatures upto 1300°C. In order to ensure that there were no air gaps between the thermocouple wire and the walls of the hole, a sodium silicate cement was used as a filler. The thermocouples were connected to a computer assisted data acquisition system.

For the water quenching experiment, the specimen was placed on a heat treatment tray and loaded in a furnace. It was then heated till the temperature in the specimen stabilized at a uniform value of 1040°C. Then, it was quickly immersed in a water tank. The water in the quench tank was agitated and the bath temperature was maintained between 14°C and 16°C throughout the experiment. As the specimen cooled, temperatures from the four thermocouples were recorded at a sampling rate of 5Hz, or,

5 data points per second, for the first 10 minutes and then at rate of 1 data point every 50 seconds (0.02Hz) for the remaining duration of the experiment. Specimen type B was heated to an initial uniform temperature of 950°C and then underwent the same procedure as type A.

For the static air cooling process, the same procedure was used to heat the specimen to a uniform temperature of 1040°C. The specimen was then removed from the furnace and placed on a minimally grilled surface in order to minimize surface-surface contact. It was then allowed to cool naturally. An initial sampling rate of 1 data point every 2 seconds (0.5Hz) was employed for the first 20 minutes following which a sampling frequency of 1 data point every 20 seconds was used for the rest of the experiment. Specimen type B was heated to an initial uniform temperature of 950°C and then subjected to the same procedure as specimen type A.

The sampling frequency used was higher in the water quench experiment due to the faster cooling rate compared to the air cool case. The sampling rate chosen should be sufficiently rapid to detect the transformation. At the same time, very high sampling rates result in data which is more prone to noise, hence greater correlation between successive observations. In all the experiments, temperature data recording was stopped when steady state cooling conditions were reached.

The water quench resulted in a direct austenite to martensite transformation and the range of temperatures over which this transformation is completed is not known exactly. More importantly, from the sampling frequency standpoint, this transformation was not depicted on the cooling curve unlike the air cool in which a gradual transformation was observed between 440°C and 480°C.

Experiments for obtaining data from surface mounted thermocouples were conducted in an identical manner. It must be said that the interior sensor locations were chosen so as to cover a wide variety of depths from the convecting surface. Sensors on the surface were located at as many positions as were thought to possess unique conditions of convection (both free and forced).

2.3 HEAT TRANSFER THEORY

In its general form, in cartesian coordinates, the following parabolic heat equation is solved to obtain the temperature distribution T(x,y,z,t).

$$\frac{\partial}{\partial x} k_x \frac{\partial T}{\partial x} + \frac{\partial}{\partial y} k_y \frac{\partial T}{\partial y} + \frac{\partial}{\partial z} k_y \frac{\partial T}{\partial z} + Q = c \frac{\partial T}{\partial t} \qquad (1)$$

$Q(x,y,z,t)$ = source or sink rate of heat in Ω (W/m^3)

k_x, k_y, k_z = thermal conductivity vector (W/mK)

c = volumetric specific heat (J/m^3)

Since k and c are functions of T, the heat equation is non-linear. The essential boundary condition may be expressed as

$$T(x,y,z) = T_1(x,y,z,t) \qquad (2)$$

on the boundary S_1 ; i.e; $(x,y,z) \in S_1 : t>0$, as shown in figure 4.

On the boundary of Ω the natural boundary condition satisfied is defined as

$$q + k_n \frac{\partial T}{\partial n} + h(T-T_0) + \sigma\varepsilon(T^4 - T_0^4) = 0 \qquad (3)$$

on the boundary S_2 ; i.e; $(x,y,z) \in S_2 : t>0$

where

k_n = thermal conductivity normal to the surface (W/mK)

$q(x,y,z,t)$ = a prescribed flux (W/m^2)

h = heat transfer coefficient for convection (W/m^2K)

σ = Stefan-Boltzmann constant (W/m^2K^4)

ε = emissivity

T_0 = ambient temperature for convection and/or radiation (K)

Finally, the initial condition must be specified for $(x,y,z) \in \Omega$:

$$T(x,y,z,0) = T_0(x,y,z) \tag{4}$$

If the partial differential equation (1) and the boundary conditions (2) and (3), and the initial condition (4) are consistent, the problem is said to be well posed and possesses a unique solution. The quenching problem was an initial value problem with the temperature at all points in the body being specified at the start of the cooling process, at 1040°C or 950°C, as the case may have been. During the FEA, radiation effects were neglected due to the marginal differences they produced in the results at enormous computational costs. Hence, according to our model, equation (3) is accurately represented as

$$q + k_n \frac{\partial T}{\partial n} + h(T - T_0) = 0 \tag{5}$$

The quarter symmetry of the specimen was used to advantage in creating a 3D finite element mesh, shown in figure 5, composed of 10-noded tetrahedral thermal solid elements. This element type is particularly suited for meshing arbitrary volumes. The finite element mesh was optimized such that the mesh density at the surfaces, where heat transfer rates are most rapid due to convection, was higher than towards the core, where heat transfer rates are slower and the temperature fluctuations damped. Likewise, time step selection was optimized to adequately represent high cooling rates at the start of cooling compared to near steady-state conditions later in the process. Particular attention, with regard to time stepping, was paid to the time range wherein the critical phase transformation temperature range was expected to lie.

2.4 RESULTS AND DISCUSSION

2.4.1 SURFACE MOUNTED THERMOCOUPLES

For the ground state model, the temperature dependent thermal conductivity and volumetric specific heat were taken from Goldak's work [5], as shown in figures 6 & 7. These were based on a 1020 steel, whose CCT diagram is shown in figure 8. The convective heat transfer coefficients for air and water were considered to be constant at their room temperature values during this first run. Comparison of the numerically obtained cooling curve with the experimental result, for a surface mounted thermocouple as shown in figure 9, indicated that the shape of the numerical curve was reasonable but the rate of temperature change was too slow in the case of the air cool model. In other words, the numerical curve would have to be shifted downwards if it were to compare more favorably with the experimental one. Further, it is evident that more solution time

steps would have to be incorporated in the transformation time range. A similar comparison for the water quench, shown in figure 10, indicated that the effective modeling of the cooling rate during the very early stages of the quench would be critical to obtaining more accurate results.

As a first iteration, temperature dependent convective heat transfer coefficient values were used for both the air cool and water quench cases. For air, the results obtained by B.Hernandez-Morales et al. [8], using inverse heat transfer techniques, was used. This is shown in figure 11. The heat transfer coefficient for water quenching with no agitation was chosen as depicted in figure 12. This variation was used by Buchmayr and Kirkaldy [11] first. A subsequent comparison of the experimental and numerical cooling curves at the center of the cavity for both the air cool and water quench cases, shown in figures 13 & 14 respectively, showed a marked improvement in the correlation between the two sets of results. In the air cool case, the main weakness of the numerical result was the temperature range over which the transformation was believed to occur, which was incorporated in the model. The water quench did not reveal any transformation behaviour and the correlation between the two sets of results was very good. This modification of the heat transfer coefficients for air and water was retained for all future FEA considering that it resulted in a better representation of the boundary conditions imposed on the finite element model rather than affecting the microstructural modeling of phase transformations.

The further iterative changes made in the modeling of the air cool case alone are now discussed. Water quenching had resulted in a direct transformation from austenite to martensite and hence the original metal thermal conductivity values were an adequate representation of this property in relation to phases present. However, the air cool had resulted in the formation of some ferrite, whose lower heat conductivity had to be accounted for. The basis for this modification rested in the experimentally generated CCT curves for the specific steel chemistry of the specimen, shown in figure 15. This CCT diagram was generated as a part of a related study on the metallurgical properties of the

steel. The superimposition of the transient temperature history from a surface thermocouple on this CCT diagram, shown in figure 16, indicated that the tranformation was possibly occuring in the temperature range of 250°C to 700°C as opposed to 500°C to 800°C, as was previously modeled. This resulted in a modification of the metal thermal conductivity variation as shown in figure 17, where the original variation in the relevant temperature regime was linearly extrapolated down to 250°C. The result of imposing this change is shown in figure 18. Comparison of numerical results from figures 13 & 18 indicates that this modification had very little effect on the FEA result. This modification was also retained while further changes in modeling of the phase transformation kinetics were considered.

Two independent modifications on the volumetric heat capacity were implemented. The first modification was essentially based on the same rationale used to modify the thermal conductivity values. In this case, the total heat capacity change associated with the transformation, as predicted by Goldak, was now spread over the 250°C - 700°C range, as shown in figure 19. It is important to note that although the shape of the curve was modified considerably, the integral over the respective temperature ranges was kept constant. Results from this iterative run, shown in figure 20, indicated that the transformation was in effect blunted by modeling the heat capacity change as a constant over an extended temperature range. Principally, the heat capacity due to the phase change had been estimated assuming the transformation products were evenly, or linearly distributed over the transformation temperature range, as shown in figure 21, resulting in a transformation"less" model in effect. This served to heighten the disparity between the experimental and numerical correlation, especially at lower temperatures after the transformation was completed.

The failure of the above modification indicated that the gap in understanding the transformation kinetics had not been filled yet. An alternate modification on the volumetric heat capacity was made. This time, the kinetics were assumed to be similar to those exhibited by an AISI 4024 steel, whose CCT diagram, shown in figure 22, was

similar to that of the steel used in this study. The expected transformation kinetics were approximated bilinearly, as shown in figure 23. This change reflects itself on the volumetric heat capacity curves as two transformation bursts, one of greater magnitude than the other, shown in figure 24. The effect of this modification on the FEA result is shown in figure 25. As it can be seen, this effect is indistinguishable from the effect of the previous modification.

At this stage, careful scrutiny of the experimental curve indicated that the transformation was occuring over a very narrow temperature range i.e; 440°C and 480°C. Thus, Goldak's estimate of the total heat capacity associated with the transformation was now concentrated over this significantly smaller temperature range, as shown in figure 26. This iteration, combined with a refinement of the finite element mesh resulted in very good agreement between the experimental and FEA results, as can be seen in figure 27.

Once the temperature dependent heat transfer coefficient values obtained from the literature were used, the FEA results for the water quench were in excellent agreement with the experimental curves, and warrant no further discussion at this stage. For the air cool case, the use of the heat transfer coefficient values found in the literature combined with a refined finite element mesh, markedly improved the correlation between FEA and experimental results. However, differences still existed. The FEA predicted rate of cooling at the start of the process was lower than observed experimentally. This suggested that the existing database for the heat transfer coefficient for air, obtained from 2D inverse analysis, was not adequately representing the convective boundary condition experienced by a complex 3D geometry such as the subject of this study. The determination of the heat transfer coefficient for this particular geometry is described in chapter 3. Another drawback of the FEA result was the inaccurate modeling of the phase transformation. This disparity could be rectified if the transformation kinetics for this specific steel chemistry are thoroughly understood.

For all future finite element analyses, the modified database of properties obtained

thus far was used.

2.4.2 EMBEDDED THERMOCOUPLES

Now that the numerical and experimental results displayed acceptable correlation for superficial locations on the specimen, the correlation at interior locations was examined. Looking at the curves for the center of the cavity section, 1" below, 3" below and 5" below, several observations can be made. First, comparing only the experimentally generated curves, shown in figure 28, it is apparent that there is an increase in cooling rate as we move form the 1" to the 3" and onto the 5" location, in that order. This change, in going from the 1" location to the 3" location, is slight compared to the increase in cooling rate observed in going from the 3" location to the 5" location. This is not surprising considering that the change in the area of cross-section in going from the 1" location to the 3" location is less than that in going from the 3" location to the 5" location.

At this point, reference shifts to figures 27,29,30,31,32. These give an idea of how well the FEA results measure up to the experimental data. The agreement between these is excellent for the 1"-below case. As one moves to faster cooling locations i.e; 3"-below and 5"-below, the agreement becomes progressively worse. In fact, looking at figures 28 and 29 indicates that the FEA solution is relatively "inelastic" in its response to the variation in the cooling conditions with decreasing cross-section. In going from the thicker to thinner cross-sections, the numerical curves show little variation in cooling rate.

Consider now figures 33 & 34. The cavity of the specimen is subjected to extremely complex heat transfer conditions due to its unusual geometry. The boundary conditions for the cavity section are not known precisely due to the possibility of the

formation of convection cells and other turbulent phenomena. To get an idea of what these conditions might be, the cooling curves for the center of the cavity section and 1"-below were compared since they appeared to be remarkably similar. This similarity was observed in both the experimentally generated curves and the FEA solution. That the FEA solutions for these to locations are very similar is not surprising due to its "inelastic" response, mentioned above. Further, only ordinary convective boundary conditions were imposed for the cavity in the finite element model. The identical nature of the experimentally generated cooling curves for these two locations is very interesting because it suggests that the effective cooling conditions at these two locations are nearly identical inspite of the differing heat transfer mechanisms at these two locations i.e; conduction at the 1"-below location and some combination of forced convection with an extended vapor blanket stage at the cavity section.

2.4.3 GENERAL DISCUSSION

The accurate calculation of the transient temperature field for a 3D steel geometry has been the main objective thus far. Air cooling characteristics observed at surface and interior locations indicate that the corresponding cooling curves may be considered in three parts i.e; the pre-transformation portion, the transformation range, and, the post-transformation portion. The accurate calculation of the temperature history in the pre- and post-transformation portions is dependent only on the accuracy with which the heat extraction conditions at the boundaries are specified and the accuracy of specification of the temperature dependency of the metal thermal conductivity. Based on the observations of the effects of the existing database for metal thermal conductivity, it seems to be adequate and applicable to a variety of low alloy steels. Since the dominant mode of heat transfer at the boundaries is convection, the temperature dependency of the convective

heat transfer coefficient has to be defined accurately. The estimation of this geometry dependent property for the specimen under study, for air, is described in chapter 3.

Consider the range of temperatures over which the phase transformations occur. The latent heat of transformations is released as an unknown function of temperature over this range. As any unit volume of the steel attains the temperature required to initiate the transformations, energy is released locally as a continuous but unknown function of temperature until the temperature falls below a critical value. These local energy releases affect temperatures at locations in and around the unit volume. The total energy released, the rate of release as a function of temperature, the temperature bounds and the volume affected are all unknown variables. Further, the effect of alloying elements on these variables is also unknown. However, this type of information is required as input data in order that accurate temperature field calculations may be made using FEA. The combined effect of these parameters is expressed in the temperature dependency of the volumetric heat capacity for each alloy. Thus, given reliable estimates for the convective heat transfer coefficient and metal thermal conductivity, it is this thermophysical property that is key to making reliable temperature history calculations over the transformation range of temperatures, using FEA. Once the transformations begin, all future temperature histories are affected irrevocably. Thus, the transformation range has to be accounted for before calculating temperatures in the post-transformation portion.

CHAPTER 3

NUMERICAL ESTIMATION OF CONVECTIVE HEAT TRANSFER COEFFICIENT FOR AIR

3.1 INTRODUCTION

If the heat flux or temperature histories at the surface of a solid are known as a function of time, then the temperature distribution associated with it can be determined. This is termed a direct problem. In many dynamic heat transfer situations, the surface heat flux and temperature histories of a solid need be determined from transient temperature measurements at one or more interior locations. This is an inverse problem.

The inverse heat conduction problem is much more difficult to solve analytically than the direct problem. But in the direct problem many experimental impediments may arise in measuring or producing given boundary conditions. The physical situation at the surface may be unsuitable for attaching a sensor, or the accuracy of a surface measurement may be seriously impaired by the presence of the sensor. Although it is often difficult to measure the temperature history of the heated surface of a solid, it is easier to accurately measure the temperature history at an interior location or at an insulated surface of the body. Thus there is a choice between relatively inaccurate measurements or a difficult analytical problem. An accurate and tractable inverse problem solution would thus minimize both disadvantages at once [12].

The problems of determining the surface temperature and the surface heat flux histories are equivalent; if one is known the other can be found in a straightforward

fashion. They cannot be independently found since in direct heat conduction problems only one boundary condition can be imposed on a given boundary at a given time. However, the heat flux is more difficult to calculate accurately than the surface temperature.

The fundamental objective of this work is to determine the convective heat transfer coefficient values for air as a function of temperature. The inverse problem has been defined as the estimation of the surface heat flux history given one or more measured temperature histories inside a body conducting heat. The temperature dependent film coefficient values for air can be determined from the transient flux history by the direct application of a simple equation. It may be noted that the word "estimation" is used because in measuring the internal temperatures, errors which affect the accuracy of the heat flux calculation are always present. Further, even if discrete data accurate to a large but finite number of significant figures are used, the heat flux cannot be determined exactly.

3.2 MATHEMATICAL MODEL FOR THE INVERSE PROBLEM

3.2.1 THE HEAT EQUATION

In its general form, in cartesian coordinates, the heat equation is a parabolic equation represented as follows.

$$\frac{\partial}{\partial x}k_x\frac{\partial T}{\partial x}+\frac{\partial}{\partial y}k_y\frac{\partial T}{\partial y}+\frac{\partial}{\partial z}k_z\frac{\partial T}{\partial z}+g(x,y,z,t)=\rho c\frac{\partial T}{\partial t} \qquad (1)$$

where :

g (x,y,z,t) is the source or sink rate in Ω, the body (W/m^3)

kx, ky, kz represent the thermal conductivity vector (W/mK)

c is the specific heat (J/kgK)

ρ is the density (kg/m^3)

$$T(x, y, z, 0) = T_0(x, y, z) \tag{2}$$

$$\frac{\partial}{\partial x} k_x \frac{\partial T}{\partial x} + \frac{\partial}{\partial y} k_y \frac{\partial T}{\partial y} + \frac{\partial}{\partial z} k_z \frac{\partial T}{\partial z} \Big|_L = h[T_\infty(t) - T(x_L, y_L, z_L)] \tag{3}$$

Equation (2) describes the initial condition and (3) defines the convection boundary at x=L

$$T(x_1, y_1, z_1, t_i) = Y_i \tag{4}$$

Y_i denotes experimentally measured temperatures.

The objective then, is to estimate the surface heat flux at discrete times, t_i , from

$$q(t_i) = \frac{\partial}{\partial x} k_x \frac{\partial T}{\partial x} + \frac{\partial}{\partial y} k_y \frac{\partial T}{\partial y} + \frac{\partial}{\partial z} k_z \frac{\partial T}{\partial z} \Big|_0 \qquad (5)$$

The thermal conductivity, density and specific heat are known functions of temperature. Hence the inverse problem is nonlinear. The volume energy source term, g, accounts for the energy contribution arising out of a phase transformation as would be the case when austenite decomposes to ferrite and/or pearlite and/or bainite and/or martensite.

3.3 EXACT SOLUTIONS OF THE INVERSE PROBLEM

Exact solutions of the inverse problem are very important because

(1) they provide closed form expressions for the heat flux in terms of temperature measurements

(2) they provide considerable insight into the characteristics of inverse problems

(3) they provide standards for comparison of approximate methods.

Inverse heat conduction problems can be categorized as steady-state or transient problems. This study involves the transient problem with a distributed thermal capacitance, which in effect, means that temperature gradients exist inside the conducting body resulting in a non-uniform temperature distribution. No exact solution to the nonlinear inverse problem of heat conduction for which the temperature sensor is at an arbitrary location inside a three-dimensional body are available in literature. Thus approximate methods have to be used.

3.4 APPROXIMATE METHODS FOR DIRECT HEAT CONDUCTION PROBLEMS

The basic concepts and methodology of approximate solutions for the direct problem form the basis of such solutions to the inverse problem also. Hence it is essential to discuss, at least briefly, these conceptual foundations.

Numerical procedures employed to solve the direct heat conduction problem fall into two broad categories. One is based on an integral formulation of the mathematical model and the other on a differential form of the model. The transient heat conduction equation can be either linear or nonlinear. For the linear case the partial differential equation formulation can be equivalently represented by an integral equation. The most important approach that employs integral equations is one using Duhamel's Theorem or Integral.

Duhamel's theorem [12] can be considered to be a result of the principle of superposition and thus is valid only for linear cases. There are several ways of deriving it, using Laplace transforms or the concept of superposition. Duhamel's theorem employs a "building block" solution which is used with the superposition principle to obtain the temperature at any spatial coordinate and time. One such solution is ϕ (r,t) which is for the temperature rise at a point $\overline{r}$ in a heat conducting body due to the heat flux,

$$q(t) = \begin{matrix} 0, & t<0 \\ 1, & t>0 \end{matrix}$$

This is called the unit step heat flux. The thermal properties of the body are independent of temperature but can be functions of position, and the temperature distribution need not be one-dimensional. The derivation requires that the surface heat flux be a product of two functions, one a function of only space coordinates and the other only of time. Duhamel's theorem, also known as Duhamel's Integral is expressed as,

$$T(\vec{r}, t) = T_0 + \int_0^t q(\lambda) \frac{\partial \phi(\vec{r}, t-\lambda)}{\partial t} d\lambda \qquad (6)$$

Equation (6) is a heat flux form of Duhamel's Integral; it is a convolution because there is a product of two functions, one of λ and the other of $t-\lambda$. There is a folding or convoluting of one function with respect to the other. A numerical approximation of equation (6) is expressed as,

$$T_M = T_0 + \sum_{n=1}^{M} q_n . \Delta\phi(\vec{r}, t_{M-n}) \qquad (7)$$

If the actual heat flux is constant over each time step, the above expression is exact for the temperature T_M ; it yields approximate results if the true heat flux varies over the time steps. The importance of this equation cannot be overstated because it gives a convenient expression for the temperature in terms of the heat flux components.

Duhamel's theorem is a powerful technique for solving a wide variety of linear heat conduction problems, but, many situations exist in which either the technique becomes too cumbersome or is not applicable. The most severe limitation is for non-linear problems with temperature dependent thermal properties. In many heat transfer problems, the temperature change of a body exposed to a heat flux is sufficiently large that the changes in thermal properties are appreciable. In these cases, the nonlinear partial differential equation of heat conduction is converted into a system of linear

algebraic equations involving the temperature at discrete locations. Two popular approaches for discretizing partial differential equations are finite differences and finite elements. Another very interesting approach involves the application of the conservation of energy for a finite control volume. The finite control volume procedure results are referred to as distributed capacitance effects because the thermal capacitance of a control volume may be distributed over several nodes. The finite difference method is also a lumped capacitance approach because the thermal capacitance associated with the entire volume is lumped at a center node point for all interior control volumes. The results from the finite element method are identical to the lumped thermal capacitance results for interior nodes.

3.5 INVERSE HEAT CONDUCTION ESTIMATION PROCEDURES

The inverse heat conduction problem is an ill-posed problem involving an estimation using data. Ill-posed problems include the mathematical problems of the solution of singular or ill-conditioned systems of linear algebraic equations, differentiation of functions known only approximately, solution of partial differential equations using "interior" measurements and solution of integral equations of the first kind utilizing measurements. In order for the problem to be well-posed it is necessary that the solution exist, be unique and be continuously dependent on the data, or equivalently, be stable. It is the condition of stability which is not met by the solution of the inverse heat conduction problem. Arbitrarily small differences in the input temperature can result in arbitrarily large differences in the surface temperature or flux.

Difference methods offer considerable potential for solving the non-linear direct and inverse heat conduction problems particularly because the non-linearity associated with temperature dependent thermal properties can easily be accomodated with difference

methods. The procedure involves local linearization of the problem by evaluating all thermal properties at temperatures corresponding to the previous time step. Thermal properties are seldom known to sufficient accuracy to justify iteration. This approach is called quasi-linearization.

At this stage, it is essential to introduce the concept of sensitivity coefficients [12]. The sensitivity coefficient associated with an unknown parameter is defined as the first derivative of a dependent variable, such as temperature, with respect to the unknown parameter, such as a heat flux component. If the sensitivity coefficients are either small or correlated with one another, the estimation problem is difficult and very sensitive to measurement errors. Thus irrespective of the problem being one of function or parameter estimation, a detailed examination of sensitivity coefficients can provide considerable insight into the estimation problem.

For the inverse heat conduction problem, sensitivity coefficients of interest are those of the first derivatives of temperature T at location x_k and time t_i with respect to a heat flux component q_M , and are defined by

$$X_{kM}(x_k, t_i) = \frac{\partial T(x_k, t_i)}{\partial q_M} \tag{8}$$

for $k=1,2,\ldots,J$, $i=1,2,\ldots,n$, and $M=1,2,\ldots,n$. The number of times t_i equals the number of heat flux components. The heat flux component q_M is the constant heat flux between times t_{M-1} and t_M. For the transient problem, such as the subject of this study, the sensitivity coefficients are zero for $M>i$. In other words, the temperature at time t_i is independent of a yet to occur future heat flux component q_M , $M>i$.

The inverse heat conduction problem is linear if the heat conduction equation is

linear and the boundary conditions are linear. The thermal properties (k,ρ,c) can be functions of spatial coordinates and not affect the linearity. They cannot, however, be functions of temperature without causing the problem to be nonlinear. One way to determine linearity is to inspect the sensitivity coefficients. If the sensitivity coefficients are not functions of the parameters, then the estimation problem is linear. If they are, the problem is nonlinear.

Two kinds of sensitivity coefficients occur depending on the nature of the approximation of the thermal flux [12]. One is due to a step q_M in the heat flux for an infinite time duration and the other, due to a pulse q_M in the heat flux for the time duration t_M-t_{M-1}. Since the duration of the step function is infinite, the step function sensitivity coefficient is expected to grow without bound. For a sensor located at depth x_k , the temperature response due to the step in heat flux can be written as

$$T(x_k, t, t_{M-1}, \bar{q}_{M-1}, q_M)$$

t_{M-1} denotes the time at which the heat flux step (or pulse) begins; $\bar{q}_1$, $\bar{q}_2$,..., $\bar{q}_{M-1}$ contain all the information about the time variation of the heat flux prior to time t_{M-1} , and hence contain all the initial temperature information necessary to continue the temperature calculations to t_M , t_{M+1},..... The step function sensitivity coefficient is defined by

$$\frac{\partial T(x_k, t, t_{M-1}, \bar{q}_{M-1}, q_M)}{\partial q_M} = Z(x_k, t, t_{M-1}, \bar{q}_{M-1}, q_M) \qquad (9)$$

where:

x_k is the sensor location

t	is an arbitrary time
t_{M-1}	is time at the beginning of the heat flux step
$\bar{q}_{M-1}$	is the previous flux history
q_M	is the magnitude of the heat flux step

For a linear problem, Z, the step sensitivity coefficient, is independent of q_M. Expressed in another way, T is a linear function of q_M. The quasi-linear application involves holding the thermal properties constant over a few future time steps while allowing some property variation over the entire time domain. For this case, Z is independent of q_M but it depends on t_{M-1} and $\bar{q}_{M-1}$ through the temperature profile at t_{M-1}. By definition, a sensitivity coefficient is identically zero prior to the initiation of the heat flux step or pulse.

The pulse sensitivity coefficient denoted by X with the same arguments as those for the step function sensitivity coefficient can be obtained from the latter by simple relationships for linear and quasi-linear problems. For linear problems,

$$Z_{k,r} = \sum_{j=1}^{r} X_{k,j} \tag{10}$$

which states that for linear problems, the response due to a step is the sum of the responses due to a series of pulses of constant magnitude and distributed over the same time interval.

For quasi-linear and constant property cases, superposition is used to calculate X from Z. For non-linear problems, the sensitivity coefficients can be calculated from differences of the temperatures at the same time and location for two values of the heat flux. For example, the temperature distribution is calculated for two different values of heat flux q^* and $q^* (1 + \varepsilon)$, where ε is a small parameter of the order of 0.001. The the sensitivity coefficient is given by

$$X(x_k, t, t_{M-1}, \vec{q}_{M-1}) = \frac{[T(x_k, t, t_{M-1}, \vec{q}_{M-1}, q^*(1+\varepsilon)) - T(x_k, t, t_{M-1}, \vec{q}_{M-1}, q^*)}{\varepsilon q^*}$$

.....(11)

The only difference in the X and Z sensitivity coefficient calculations is the boundary condition imposed in calculating them.

For X, the boundary condition is

$$q(T) = \begin{array}{l} q^*,\ t_{M-1} \le t \le t_M \\ 0,\ \text{all other } t \end{array}$$

For Z, the boundary condition is $q(t) = q^*$, $t \ge t_{M-1}$.

The evaluation of the above equation requires two different temperature calculations i.e; direct solutions.

The sensitivity coefficients described above in such detail are essential inputs in determining the flux history. The nature of the flux boundary condition imposed on a body at any time affects the temperature at all points in the body for all future times. This is reflected in that the sensitivity coefficient associated with a heat flux pulse of finite duration can be nonzero after the heat flux itself returns to zero. These effects are more apparent closer to the boundary while the effects and interior locations are damped and lagged. Hence while evaluating the flux going into or coming out of a body at a given point in time, its effects at future times should also be incorporated to obtain a more accurate picture. An interior location closer to the flux boundary holds more reliable or "first-hand" information about the flux than a point farther removed from the surface.

The actual steps involved in the determination of the flux history depend on the number of sensors from which data is used and the number of future time steps from which the temperature data for each of these sensors is used. In either case, discrete

transient temperatures from the sensors are used to determine the surface heat flux as a function of time. When a single sensor is used, the calcuated temperatures are made equal to the measured values. This is called "exact matching". In this case, a single temperature sensor is considered to be located at a depth x_k below the active surface. The heat flux value q_M, considered constant over the time interval $t_{M-1} \leq t \leq t_M$, that forces a matching of the computed temperature with the measured temperature at x_k. For realistic temperature data containing errors, this approach is known to produce significant oscillations in the computed heat flux. Exact matching can be obtained using a numerical form of Duhamel's integral or a finite control volume (or finite difference or finite element) method. This formulation is linear in the unknown heat flux and hence we limit its discussion to this stage.

Multiple temperature sensors are recommended in order to obtain as much experimental information as possible. However, only one sensor can be matched exactly. In order to accomodate the over-specification of the problem, a value of q_M, constant over $t_{M-1} \leq t \leq t_M$, is determined such that the least squares error accumulated over all sensors is minimized. This is called "approximate matching". The procedure involved in the solution of the multiple sensor, single future time step inverse problem is to treat each sensor independently (over a single time step) and determine the heat flux $\tilde{q}_{k,M}$ that exactly matches the single data point $Y_{k,M}$. After evaluating these for each sensor, the $\tilde{q}_{k,M}$ heat flux values are weighted according to an equation of the form

$$\hat{q}_M = \sum_{k=1}^{J} w_k \tilde{q}_{k,M} \qquad (12)$$

where w_k is the weighting function.

Based on considerations mentioned above, the sensors closest to the active surface will have the largest sensitivity coefficients and hence will automatically be weighted more

heavily.

It has already been mentioned that a flux $q(t)=q_M$, constant over $t_{M-1} \leq t \leq t_M$ and zero otherwise, will influence sensor measurements Y_M, Y_{M+1},..... Hence, it is a logical step to use these future temperature measurements to estimate q_M. Beck [12] was the first to recognize the importance of future temperature information and apply it to the Duhamel theorem solution of the inverse problem. Beck et al. [12] applied sensitivity coefficient concepts and substantially reduced the number of computations required for difference methods with future temperatures.

Now, consider the case where data from a single sensor is used and the flux is specified as a constant over an arbitrary number of future time steps. Suppose the inverse problem has been solved upto time t_{M-1} i.e; the estimated heat flux $\hat{q}_{M-1}$ and the entire temperature field at time t_{M-1} is known. In order to estimate the unknown flux q_M at time t_M, a constant value of flux is specified over 'r' future time steps such that the least squares error between the computed and measured temperatures is minimized. Alternatively, a linear or higher order flux variation may be specified over the 'r' future time steps. The least squares function is

$$S=\sum_{i=1}^{r} [Y(x_k, t_{M+i-1}) - T(x_k, t, t_{M+i-1}, \bar{q}_{M-1}, q_M)]^2 \qquad (13)$$

Differentiating S with respect to q_M, replacing q_M by $\hat{q}_M$, and setting it to zero yields,

$$\frac{\partial S}{\partial q_M} = -2\sum_{i=1}^{r} [Y(x_k, t_{M+i-1}) - T(x_k, t, t_{M+i-1}, \bar{q}_{M-1}, q_M)] \cdot X_{k,i} = 0 \qquad (14)$$

where the sensitivity coefficient is defined by

$$X_{k,i}=\frac{\partial T(x_k,\, t_{M+i-1},\, t_{M-1},\, \vec{q}_{M-1},\, q_M)}{\partial q_M}=X(x_k,\, t_{M+i-1},\, t_{M-1},\, \vec{q}_{M-1}) \qquad (15)$$

Since q_M is assumed constant over 'r' future time steps, the Z sensitivity coefficient is used instead of X.

The temperature field T (x,y,z,t) depends in a continuous manner on the unknown heat flux q_M. For the general case, this dependence is written as T (x_k, t, t_{M-1}, $\overline{q}_{M-1}$, q_M) where $\overline{q}_{M-1}$ is the vector of all previous heat flux values and t_{M-1} indicates the time that the heat flux step begins. Because the temperature field is continuous in q_M, it can be expanded in a Taylor series about an arbitrary but known value of heat flux q^*, as shown below.

$$T(x_k,\, t_{M+i-1},\, t_{M-1},\, \vec{q}_{M-1},\, q_M)=T(x_k,\, t,\, t_{M-1},\, \vec{q}_{M-1},\, q^*)$$

$$+(q_M-q^*)\,\frac{\partial T(x_k,\, t,\, t_{M-1},\, \vec{q}_{M-1},\, q_M)}{\partial q_M}\Big|_{q_M=q^*}+\frac{(q_M-q^*)^2}{2!}\,\frac{\partial^2 T(x_k,\, t,\, t_{M-1},\, \vec{q}_{M-1},\, q_M)}{\partial^2 q_M}$$

+ (higher order terms)..... .....(16)

For linear problems, only the first derivative is non-zero. Applying a similar Taylor series expansion and neglecting derivatives of order 2 and above, we get the simplified expression

$$T(q_M) = T(q^*) + (q_M - q^*) \cdot X(q_{M-1}) \qquad (17)$$

The arguments have been simplified for clarity. Substituting (16) in (14) and solving for $\hat{q}_M$ gives

$$\hat{q}_M = q_M^* + \frac{\sum_{i=1}^{r} (Y_{k,M+i-1} - T^*_{M+i-1}) \cdot X_{k,i}}{\sum_{j=1}^{r} X_{k,j}^2} \qquad (18)$$

If the thermal property variation with temperature is treated in a quasi-linear manner, Z has to be recalculated for each value of q_M i.e; each time step. The subscript k serves as a reminder that the sensitivity coefficients depend on the sensor location. The computed heat flux q_M is retained only for the time interval $t_{M-1} \leq t \leq t_M$ and a new heat flux is calculated for each subsequent time interval.

When we consider multiple sensors and an arbitrary number of future time steps for the analysis, the least squares error function must be modified to include a summation over the number of sensors. For J sensors and r future time steps, this function is defined as

$$S=\sum_{k=1}^{J}\sum_{i=1}^{r}\left[Y(x_k, t_{M+i-1}) - T(x_k, t, t_{M+i-1}, \vec{q}_{M-1}, q_M)\right]^2 \qquad (19)$$

Once again, the value of q_M, constant over r future time steps, that minimizes S is sought. The final expression for the estimated heat flux is

$$\hat{q}_M = q_M^* + \sum_{k=1}^{J}\sum_{i=1}^{r}\left[Y_{k,M+i-1} - T^*_{k,M+i-1}\right] \cdot K_{k,i} \qquad (20)$$

where

$$K_{k,i} = \frac{Z_{k,i}}{\sum_{k=1}^{J}\sum_{i=1}^{r} Z_{k,j}^2} \qquad (21)$$

Upto this point, all the function specification methods have utilized the (temporary) assumption of a constant heat flux. As mentioned earlier, other assumed functional forms can be utilized.

3.6 NUMERICAL PROCEDURE AND EXPERIMENTATION

The solution to the inverse heat conduction problem is very sensitive to measurement errors. The more information one tries to extract from the experimental data, the more pronounced is this sensitivity. Hence, a compromise has to be reached between accuracy and the amount of information used to solve the problem.

The scheme utilized to estimate the transient flux history and the convective heat transfer coefficient thereof utilized temperature data from three interior sensors over three future time steps. The three locations were chosen to be the 1"-below, 3"-below and 5"-below positions, described in section 2.2 and shown in figure 2. The step-wise algorithm to sequentially estimate the flux history with the constant heat flux assumption, three sensors and three future time steps can be described as follows.

1. Impose two flux boundary conditions $q(t) = q^*$ and $q(t) = q^*(1 + \varepsilon)$ over $t_{M-1} \leq t \leq t_{M+2}$ independently on the finite element model and perform the FEA.
2. Calculate the pulse sensitivity coefficients (X) using the difference equation i.e; equation (11). These are nine in number corresponding to each possible combination of sensor location and future time step.
3. Calculate the gain coefficients, given by equation (21). J=r=3 in this case.
4. $\hat{q}_M$ is retained, M is increased by one and the procedure is repeated.

Once the flux history is calculated in this manner, the convective heat transfer coefficients are calculated using a simple interpolative equation given by

$$\hat{h}_M = \frac{\hat{q}_M + \hat{q}_{M+1}}{2\,(T_f^M - \hat{T}_s^M)} \qquad (22)$$

where:

T_s^M = estimated surface temperature, and

T_f^M = surrounding fluid temperature.

In order to start solving the inverse problem, an estimate was needed for the flux boundary conditions to be imposed on the finite element model which would produce the same spatial temperature distribution in the model after a predetermined value of elapsed time, as was observed in the real quenching process. The basis for comparison was the transient thermal histories obtained from three sensors located in the interior of the body at 1", 3" and 5" below the surface of the cavity and along the axis of symmetry. Conceptually, this is the implementation of the "approximate matching" procedure. As a first estimate, the heat content of the body at the start of the cooling process was evaluated using the formula

$$Q = \int_{25}^{1040} m . C_p . dT \qquad (23)$$

where $C_P(T)$ is the volumetric specific heat of the material as function of temperature. The limits of integration denote the temperature from which the body is cooled i.e; 1040°C and the equilibrium steady state temperature it eventually reaches i.e; 25°C. Since a quarter symmetry model was considered, one fourth of the total mass was used for the calculation of Q.

In order to impose flux boundary conditions, the quantity of heat calculated above has to be divided by an area factor and a time factor. Based on the simplifying assumption that the outgoing flux from all the surfaces is the same, Q was divided by the total surface area of the quarter symmetry model. Now, the choice of the time factor

could have been made in several ways. The simplest and least realistic approach is to assume that the quantity of heat, Q, is dissipated via the convecting surfaces at a constant rate over the entire duration of the cooling process, in which case the time factor is the total time of cooling. In reality, however, the quantity of heat dissipated from a given surface varies continuously as a function of time in a nonlinear fashion, with decreasing quantities of heat being dissipated over identical intervals of time as cooling proceeds. Hence, in the limit, only a fraction of this initial heat content is dissipated over a very small interval of time. This fraction is definitely geometry dependent. Given the complex 3D geometry of the model, there is no way of calculating the different values of heat fluxes emanating from the different surfaces analytically. It can only be said that guesses can be made about the fraction of heat that might be dissipated over some arbitrarily small interval of time for an arbitrary geometry. Hence, an initial trial value of -9000 W/m^2 was imposed on all the convecting surfaces and the actual "averaged" flux value was determined iteratively to be -143000 W/m^2. This value of flux, when imposed on the finite element model, produced a temperature distribution that matched very closely the experimentally observed values 20 seconds after the start of cooling.

It was mentioned earlier that utilizing a higher sampling rate to obtain a greater volume of experimental data also implied greater errors in the estimated fluxes. At the same time, the greater the sampling rate, the more closely one is tracking the actual cooling process. Revisiting the definition of sensitivity coefficients discussed in section 3.5, they are defined as the partial derivative of temperature with respect to the particular flux component at a specific point in time. Each time step has a flux component assocaiated with it and hence a matching sensitivity coefficient. They are therefore indicators of how sensitive the numerical model is in its temperature response to variations in the imposed flux boundary conditions. The greater the value of sensitivity coefficients and the more consistently reproducible these are, the better the numerical model. A sensitivity coefficient of zero would indicate that the numerical model is highly insensitive in its response. It is also obvious that a greater variation in temperature

response will be observed if we impose more divergent values of flux boundary conditions. This naturally implies larger moduli of sensitivity coefficients. In the cooling process, a more accurate tracking of the flux variation over time would involve a higher sampling rate of temperatures over time. The closer in time that temperatures are recorded, the nearer in magnitude are the fluxes that caused them and hence the lower the sensitivity coefficient moduli, which is undesirable. This leads to a question about where to make the trade-off between sampling rate and accuracy. If a more detailed representation of the flux history over the time domain is desired, the sensitivity coefficient moduli are smaller and some accuracy is forgone. By opting for a coarser representation over the time domain, some accuracy is gained. Once the exact discretization of the time domain is decided upon, the values of the sensitivity coefficients are fixed.

In order to get an idea of how the sensitivity coefficients varied with the degree of temporal discretization and sensor location, a series of numerical experiments were conducted on the finite element model. All these used the function specification method with three future time steps and three sensors. Estimates for the flux at the end of 30s from the start of the cooling process were obtained using four different discretization schemes. These were

i) estimate of the flux at t=30s from the estimates for t=0s and t=10s i.e;using a 20s time interval (0-10-30-50-70).

ii) estimation of the flux at t=30s from the estimates for t=0s and t=20s i.e; using a 10s time interval (0-20-30-40-50).

iii) estimation of the flux at t=30s from the estimate for t=0s alone i.e; using a 30s time interval (0-30-60-90).

iv) estimation of the flux at t=30s from the estimates for t=0s, t=10s and t=20s i.e; using 10s time intervals with all the intermediate time steps (0-10-20-30-40-50).

The results of these test runs are shown in figures 35-40. Several observations can be made from figure 35. First, the values of the sensitivity coefficients increase and have

finite values upto the third future time step for each case i.e; 50s, 70s, 90s as the case may be. As we move towards coarser time discretization i.e; 10s to 20s to 30s, the magnitude of the sensitivity coefficients increase. Discretizing the time domain in 10s results in some of the sensitivity coefficients assuming values of 0 (cases ii and iv). Comparison of these two cases indicate that the sensitivity coefficient values for either case are almost identical. This suggests that the estimation of the flux at t=30s is dependent mainly on the estimated flux at the previous time step (t=20s in this case), which is used as input data. In other words, if the time domain is discretized in 10s intervals, there is little use in estimating the flux at t=10s. A coarser time discretization can be used and some accuracy gained in the process by estimating the flux at t=20s directly, which may then be used as input to determine the flux at t=30s. Comparison of cases i and ii indicates that the magnitude of the sensitivity coefficients are higher for case i. Based on the belief that a higher magnitude of sensitivity coefficients indicates a more accurate scheme, it can be concluded that the flux at the end of t=30s is more accurately determined from the flux at the end of t=10s than from the flux at the end of t=20s.

Comparison of the values of the flux estimates from the four schemes, figure 36 reveals an approximately 4% variation in the predicted values. Cases ii and iv are associated with almost identical values of sensitivity coefficients and hence are expected to generate similar estimates for the flux at the end of t=30s. This is indeed the case. The two estimates differ by only 0.4%. Comparing the magnitudes of the sensitivtiy coefficients for cases i and iii, we find that they are considerably different. Yet, their estimates for the flux at the end of t=30s differ by only 0.3%. This leads to an important conclusion that the magnitude of the sensitivity coefficients do not entirely affect the estimated value of flux. The above observation indicates that the solution has achieved some stability.

Consider figures 37 to 40, showing the sensor location effects. All the schemes show the same broad trends. The magnitude of the sensitivity coefficients is highest for

the sensor located 5" below the box section and minimum for the sensor located 1" below. This would suggest that the information from a sensor located at a faster cooling point in the body is more reliable than the information obtained from a sensor experiencing a slower cooling rate. This further suggests that if the fluxes were to be determined at three positions on the surface corresponding to the three interior sensor locations, the flux at the fastest cooling location will always be determined most accurately. This seemingly contradicts the intuitive expectation that a flux varying more gently over time will be easier to track down compared to a more rapidly varying flux. However, it should be remembered that the sensitivity coefficient magnitudes indicate how quickly and accurately the finite element model of a heat conducting body can mimic the real life situation in the response to a changing flux boundary condition. A thinner section has a faster cooling rate rate and hence the rate of change of temperature and the magnitude of that change is higher. The sensitivity coefficient magnitudes are thus higher. In the time domain, the passage of a greater period of time implies a greater change in temperature i.e; the response is more easily visible and therefore is associated with a higher sensitivity coefficient magnitude. Hence the notion of sensitivity coefficient magnitudes being an indication of the accuracy of a scheme has to be carefully reconsidered.

Further examination of the figures showing sensor location effects reveal that the variation of the sensitivity coefficients between any two time steps is linear. Also, the greater the duration of time for which the problem is solved, the more linear does the entire variation become. To clarify this statement, compare the curves for the 0-10-20-30-40-50 case with the 0-10-30-50-70 and 0-30-60-90 cases for any given sensor location. For the 0-...-50 case, the slope of the sensitivity coefficient variation between any two time steps keeps changing perceptibly. For the 0-...-70 case, there is only a marginal change in slope after t=30s and in the 0-...-90 case, almost no change is perceptible. Further, in each case, the variation in slope becomes more apparent for a slower cooling sensor location. This can be explained as follows. At a slower cooling sensor location,

the effects of the variation of fluxes at the surface, are damped and lagged. In fact, this is true for any interior location but the degree of damping and lagging increases as one moves further away from the surface, where all the primary changes are occuring. Hence, we expect that for sensors located at more rapidly cooling locations, the sensitivity coefficient magnitudes are higher and vary at a faster rate too. This is contrary to the observation made in the figures. The figures seem to suggest that the FEA solution is more accurate in tracking milder temperature variations as compared to quicker changes.

Recalling the definition of the sensitivity coefficient, Z,

$$Z = \frac{T[q^*(1+\varepsilon)] - T[q^*]}{\varepsilon q^*} \qquad (24)$$

The denominator of the above equation is constant with respect to time. As cooling proceeds, the rate of drop in temperature i.e; the cooling rate, decreases since the temperature gradient between the body's surface and the surrounding fluid, which acts as the driving force, decreases. Hence, for times t_1, t_2 and t_3 ($t_1 < t_2 < t_3$), we expect that the drop in temperature varies as

$$[\ T(t_1) - T(t_2)\ ] > [\ T(t_2) - T(\ t_3)\ ]$$

This is a reasonable expectation since the rate of cooling between t_1 and t_2 is faster than between t_2 and t_3. Hence the rate of increase of the sensitivity coefficient should decrease with time as shown in figure 41. This effect is carried over to the flux estimation process, as can be observed in the figure showing the flux estimates from the four schemes. The drop in flux magnitude is expected to decrease with each subsequent time step whereas the opposite trend is observed.

3.7 RESULTS AND DISCUSSION

Based on the results of the numerical experimentation and the choice of the degree of continuity with which the convective heat transfer coefficient is to be represented as a function of temperature, the inverse problem was solved for every 20s time interval during the initial stages of the cooling process. This degree of temporal discretization was maintained until the cooling rate dropped below one degree per second, approximately. This roughly translates to a 20° drop in temperature with every solution step, during which time a constant flux is assumed to emanate from all the convecting surfaces of the specimen. As the cooling process approached steady state conditions, coarser time discretization was employed since the variation in the flux became more predictable. The estimated flux history as a function of estimated surface temperature at some locations on the surface of the specimen, is shown in figure 42. This is merely a plot of the uniform flux that is assumed to emanate from every unit area on the surface of the body with temperatures at three sample surface locations. It is known, however, that the flux emanating from different parts on the surface of an arbitrary geometry is in general different. Unique flux losses at different superficial locations result in unique temperatures at those positions. Figure 42 reveals the degree of variation that may be expected in the actual flux boundary condition as we move from thicker to thinner sections. Figure 43 is a similar plot of the estimated convective heat transfer coefficient for air , h, for the specimen geometry under study. It may be noted the temperature dependency was estimated from 1040°C to 490°C, approximately. Comparison of figures 42 and 43 clearly indicates that the variation of h follows the variation of the flux history identically. This is not surprising considering a linear interpolation formula was used to calculate the convective heat transfer coefficient from the flux history. Since the transient flux history was determined by an averaging process involving temperatures at three sensor locations at different depths from the cavity section, the variation of h is

represented as a function of the average of temperatures at three analogous surface locations, as shown in figure 44.

The estimated temperature dependent convective heat transfer coefficient for air was now incorporated in the database, replacing the dependency used thus far (figure 11). Once again, the measured and the FEA predicted transient temperature histories at various locations were compared, as shown in figures 45-51. In the temperature range for which h was estimated i.e; 1040°C to 490°C, the agreement is excellent. This is particularly so for the locations experiencing slower cooling rates, namely, the cavity section, 1"-below and 2"-below positions. Further, the disparity between the two sets of results for locations experiencing more rapid cooling has markedly dropped compared to previous predictions. As mentioned earlier, this disparity exists because of the averaged sense in which h was estimated. In order that the boundary conditions at the faster cooling locations be represented exactly, the same inverse scheme, using temperature data from the 3"-below, 5"-below and tip locations alone may be used to estimate h for this portion of the specimen. Continued efforts are in progress to extend the temperature dependency of the convective heat transfer coefficient to room temperature.

The most important conclusion that may be arrived at from this work is that the inverse heat transfer method may be used to estimate the temperature dependency of the convective heat transfer coefficient for any 3D geometry. This thermophysical property is most critical in affecting the accuracy of transient thermal history calculations using FEA at all temperature ranges barring that during which phase transformations occur. The inverse method may also be applied to any quenching medium. The method however, is computationally intensive.

CHAPTER 4

CONCLUSIONS

Based on the results of this study, it may be concluded that the transient temperature field for a complex 3D steel geometry can be predicted with reasonable accuracy using FEA. Three constituents of the database of thermophysical properties were examined closely and their effects quantified. Amongst these, it is seen that the temperature dependent thermal conductivity plays only a marginal role in calculating the transient thermal histories. For this property, the database developed during this research program is quite adequate and may seemingly be applied to a wide variety of steel compositions. In essence, the metal thermal conductivity of steels seems to be a "macroscopic" property whose value does not vary significantly as the proportions of the different constituent phases change.

The use of inverse heat transfer techniques to estimate the temperature dependent convective heat transfer coefficient for air indicates that boundary conditions governing heat flow in complex 3D geometries may be accurately established. This ensures accurate temperature field calculations. The inverse method may be used for any quenching medium, like water, which is commonly used in the heat treatment industry. Numerical schemes that mimic processes more realistically may be used. For example, the complex geometry may be discretized into several lumped bodies and a linearly varying flux may be assumed to emanate from the convecting surfaces in the time elapsed between each solution step. This would isolate and account for the effect of geometry on the resultant microstructure in a steel specimen more accurately. This could be considered for future for future work.

The parameter that remains an enigma is the temperature dependent volumetric heat capacity, particularly so for the air cool case. The direct transformation of austenite to martensite during a water quench is considerably simpler to model. Information about the kinetics and energy of phase transformations is cradled in the variation of this property over temperature. It is this information that has to be available as input for the predictive model. The energy releases as a function of temperature can potentially be determined experimentally using a Differential Scanning Calorimeter.

The prediction of the transient temperature field is in general better for slower cooling locations. In order that the predicted thermal history is accurate at all locations, portions of the specimen experiencing significantly different cooling rates can be modeled separately to determine exact boundary conditions at those locations. This aspect may be considered as a modification for future work. The convective heat transfer coefficient values determined at locations with slower cooling rates can be expressed as functions of the temperature history at the more rapidly cooling part, for example, and this dependency imposed as the boundary condition there. This would involve the representation of different convective boundary conditions at different areas on the surface of the finite element model of the specimen. Implementation of this type of boundary condition would significantly increase the computational intensity of the analysis.

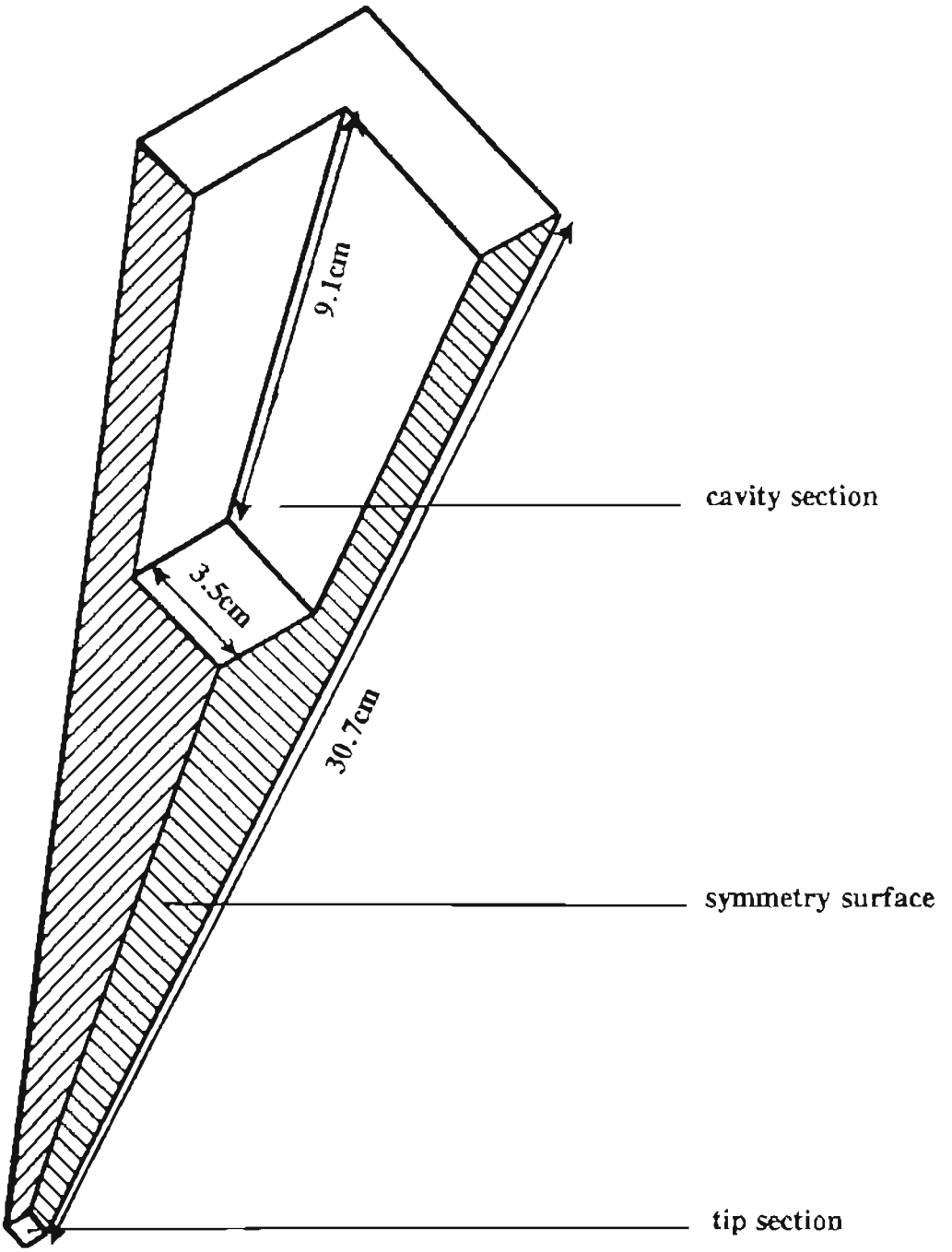

Figure 1. Quarter symmetry model of the specimen.

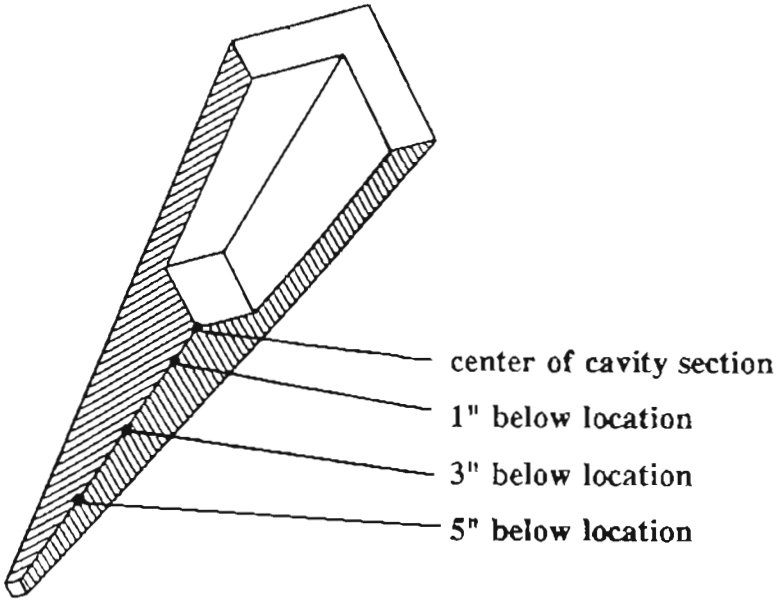

Figure 2. Specimen type A.

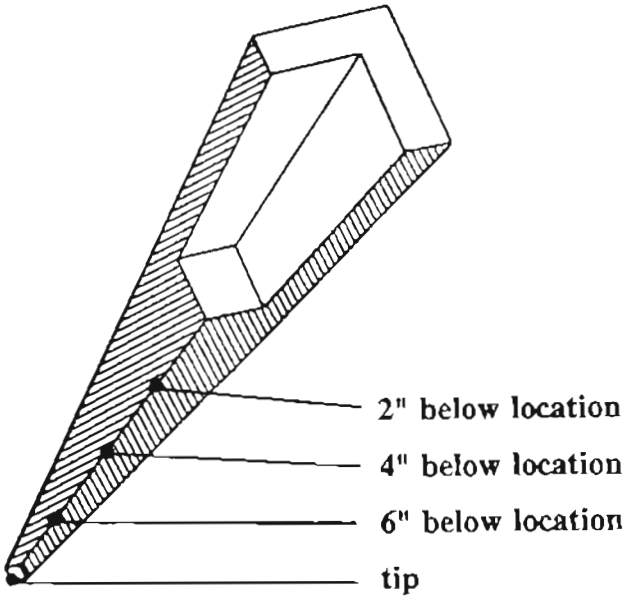

Figure 3. Specimen type B.

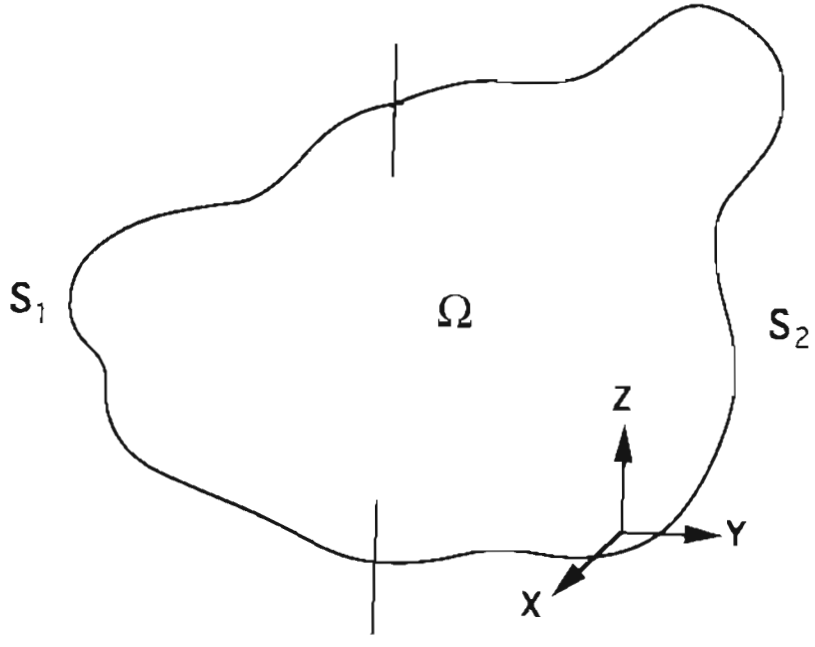

Figure 4. Domain and boundaries where situations described by equations 1-4 in chapter 2, exist.

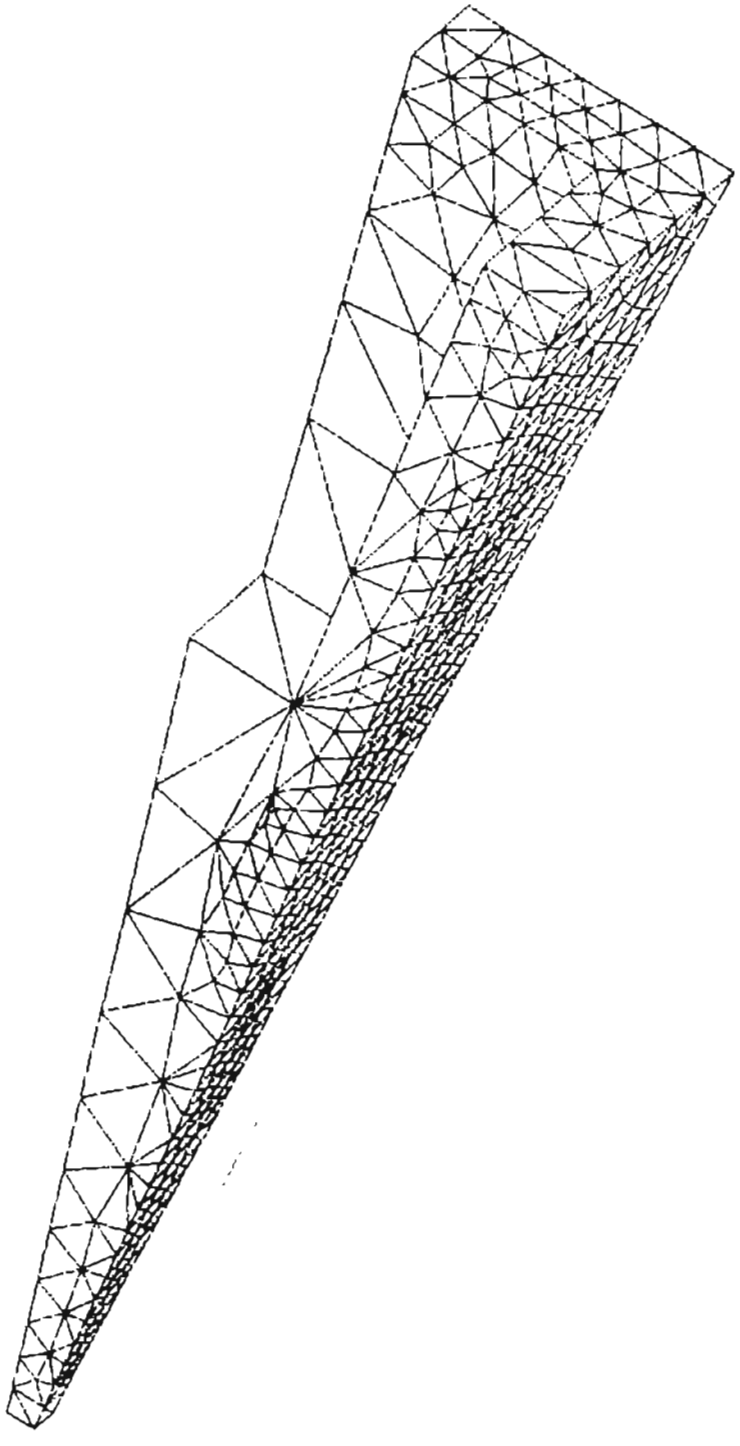

Figure 5. Finite element mesh of the quarter symmetry model.

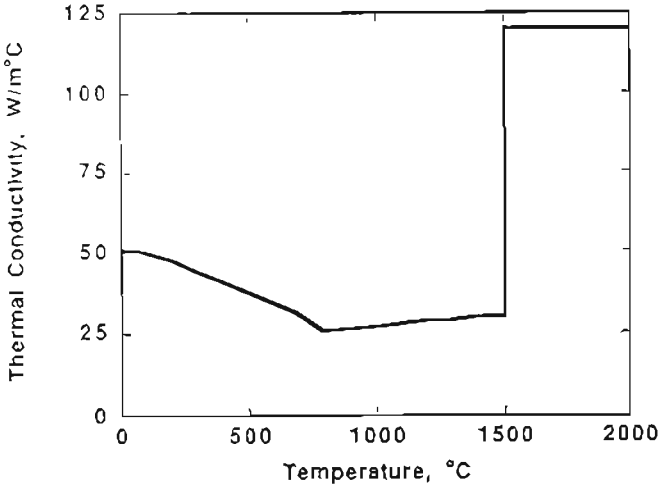

Figure 6. Temperature dependency of the thermal conductivity used in the FEA [5].

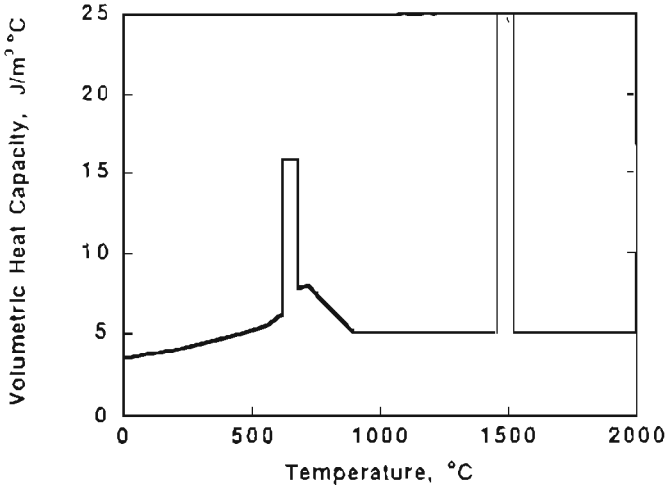

Figure 7. Temperature dependency of the volumetric specific heat capacity used in the FEA [5].

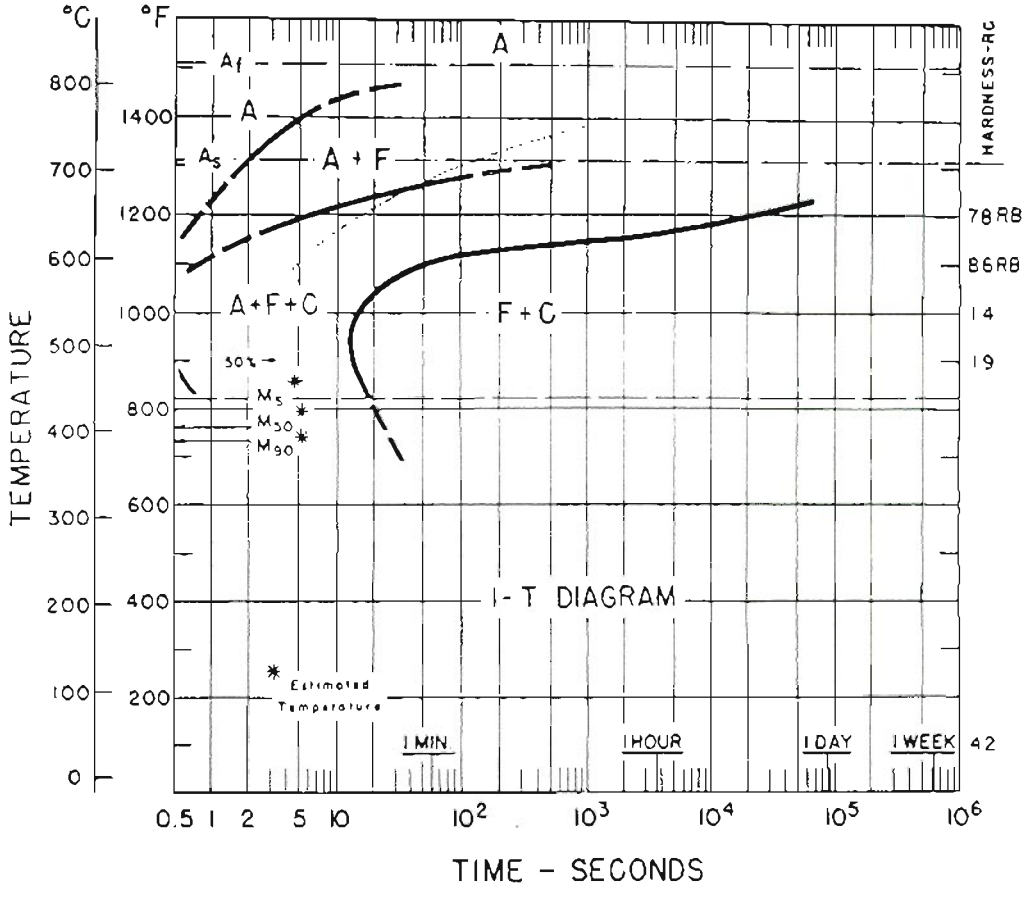

Figure 8. CCT diagram for AISI 1020 steel.

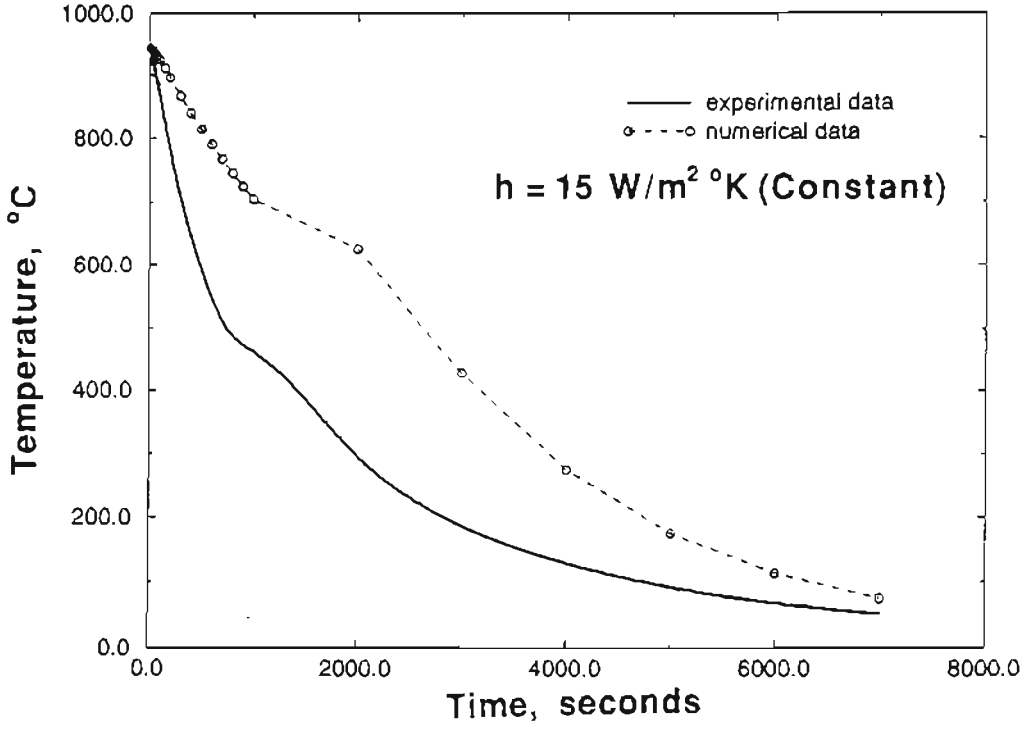

Figure 9. Comparison between measured and FEA calculated cooling characteristics at the center of the cavity section; Goldak's [5] properties used in the FEA; air cooled from 950°C.

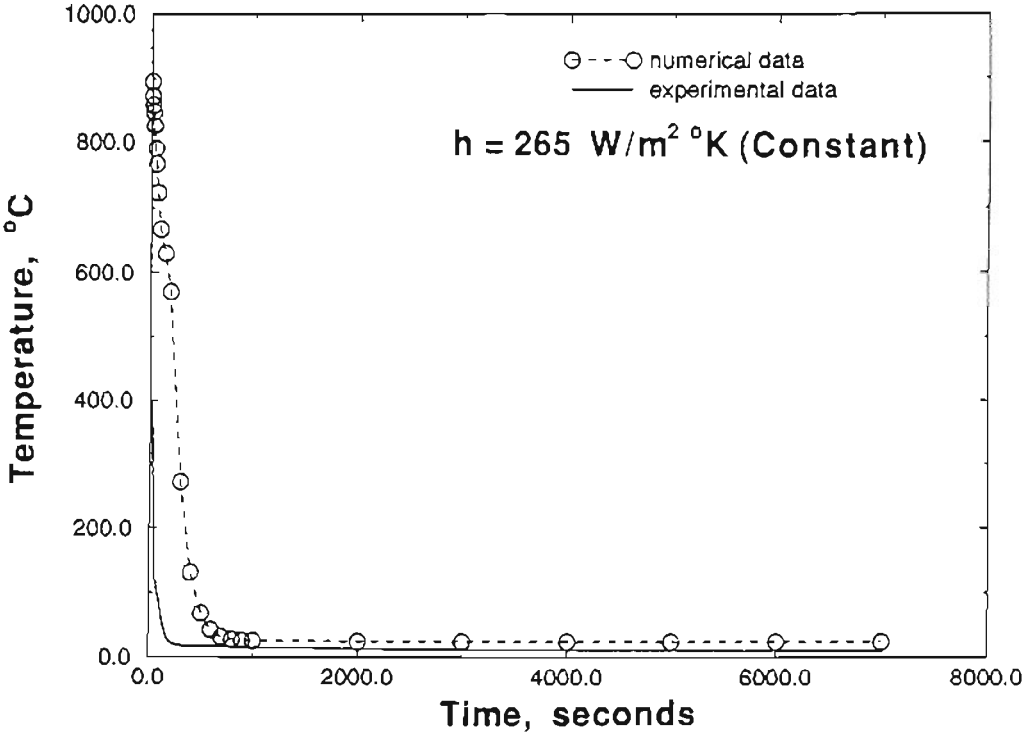

Figure 10. Comparison between measured and FEA calculated cooling characteristics at the center of the cavity section; Goldak's [5] properties used in the FEA; water quenched from 950°C.

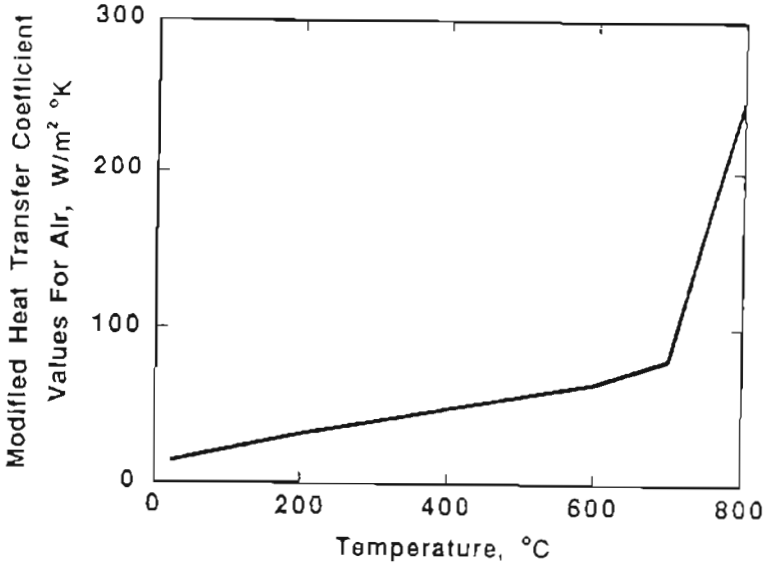

Figure 11. Temperature dependency of convective heat transfer coefficient for air used in the FEA [8].

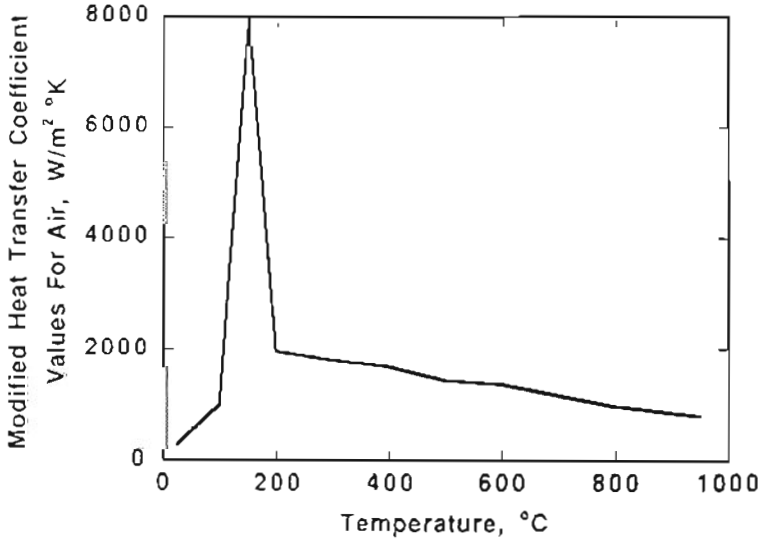

Figure 12. Temperature dependency of convective heat transfer coefficient for water used in the FEA [11].

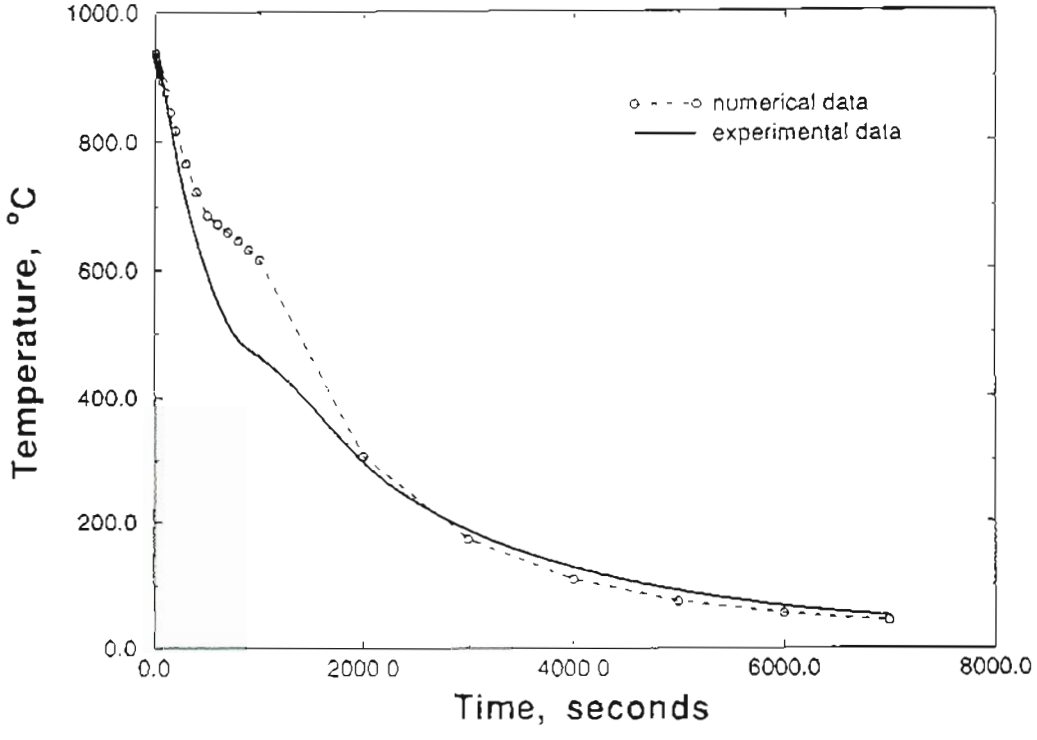

Figure 13. Comparison between measured and FEA calculated cooling characteristics at the center of the cavity section; temperature dependent convective heat transfer coefficient used in the FEA; air cooled from 950°C.

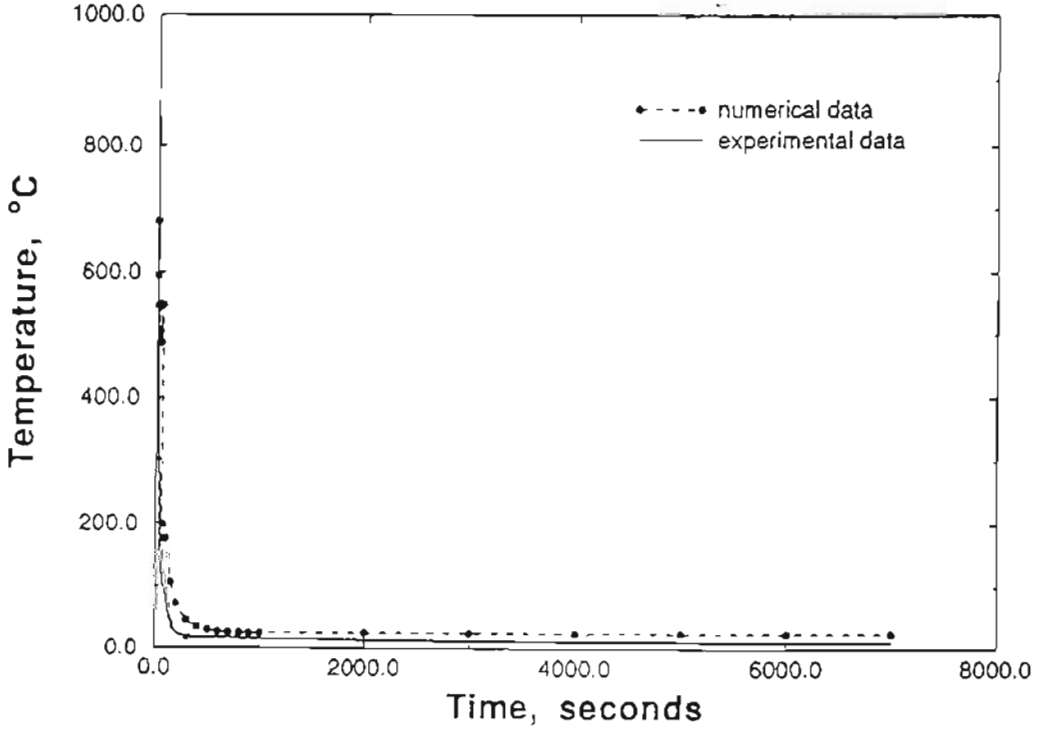

Figure 14. Comparison between measured and FEA calculated cooling characteristics at the center of the cavity section; temperature dependent convective heat transfer coefficient used in the FEA; water quenched from 950°C.

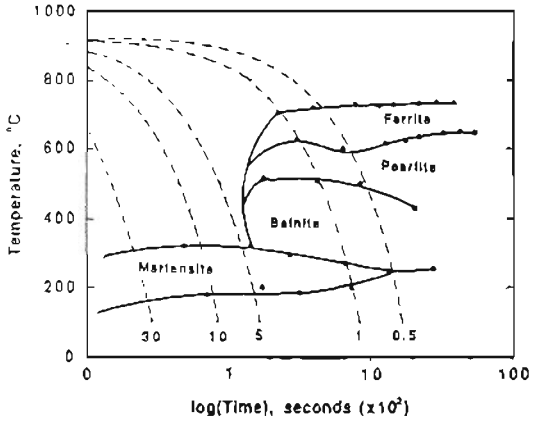

Figure 15. Experimentally determined CCT diagram for specimen steel chemistry.

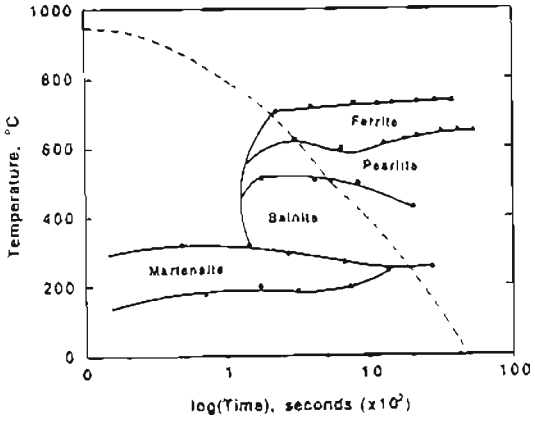

Figure 16. Measured cooling curves superimposed on experimentally determined CCT diagram for specimen steel chemistry.

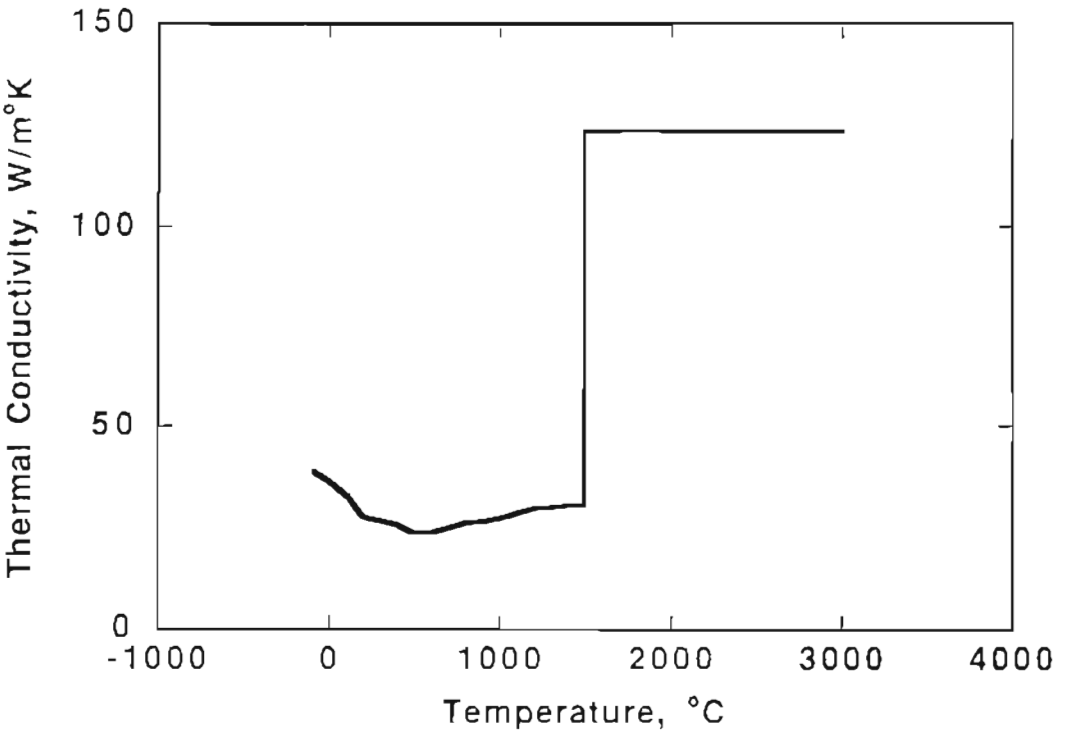

Figure 17. Modified temperature dependency of thermal conductivity used in the FEA.

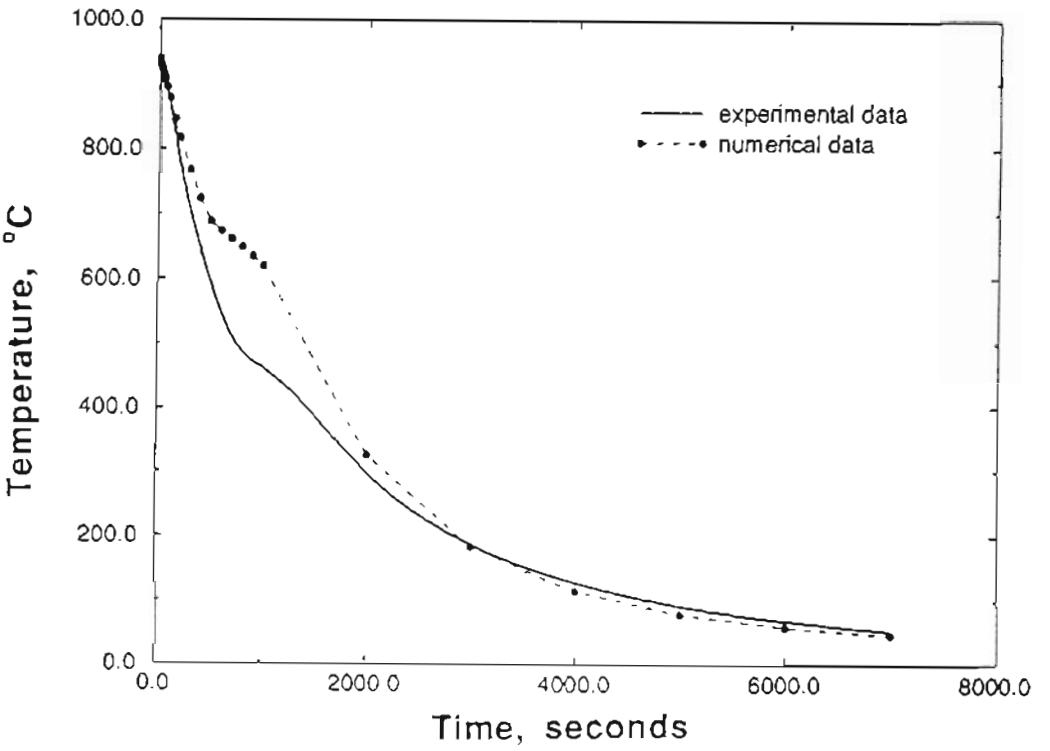

Figure 18. Comparison between measured and FEA calculated cooling characteristics at the center of the cavity section; modified temperature dependency of thermal conductivity; air cooled from 950°C.

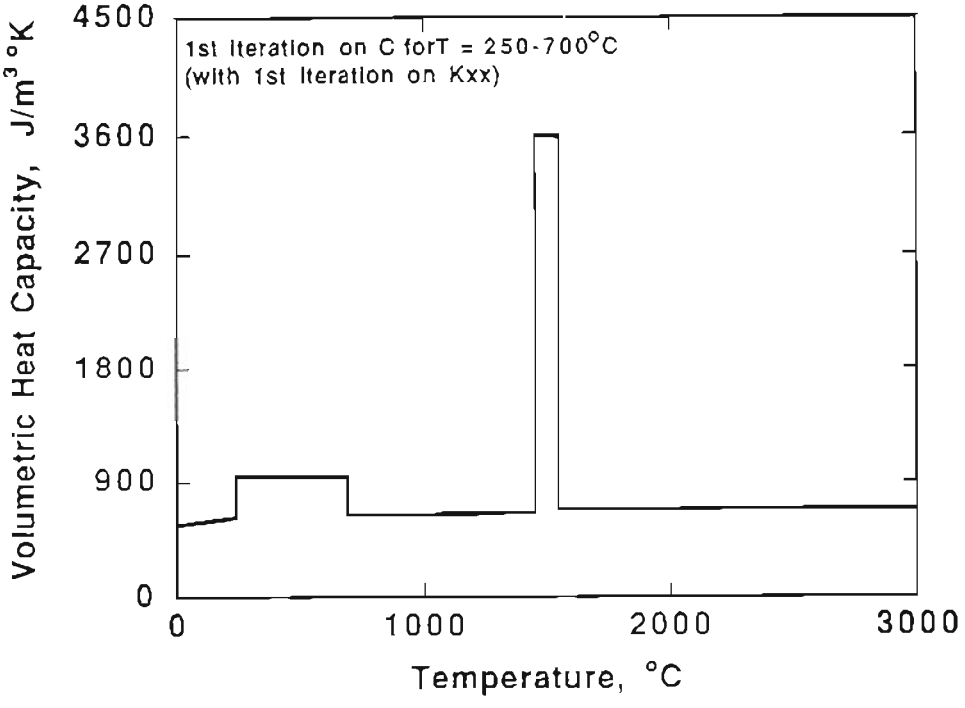

Figure 19. First modification of the temperature dependency of the volumetric specific heat capacity used in the FEA.

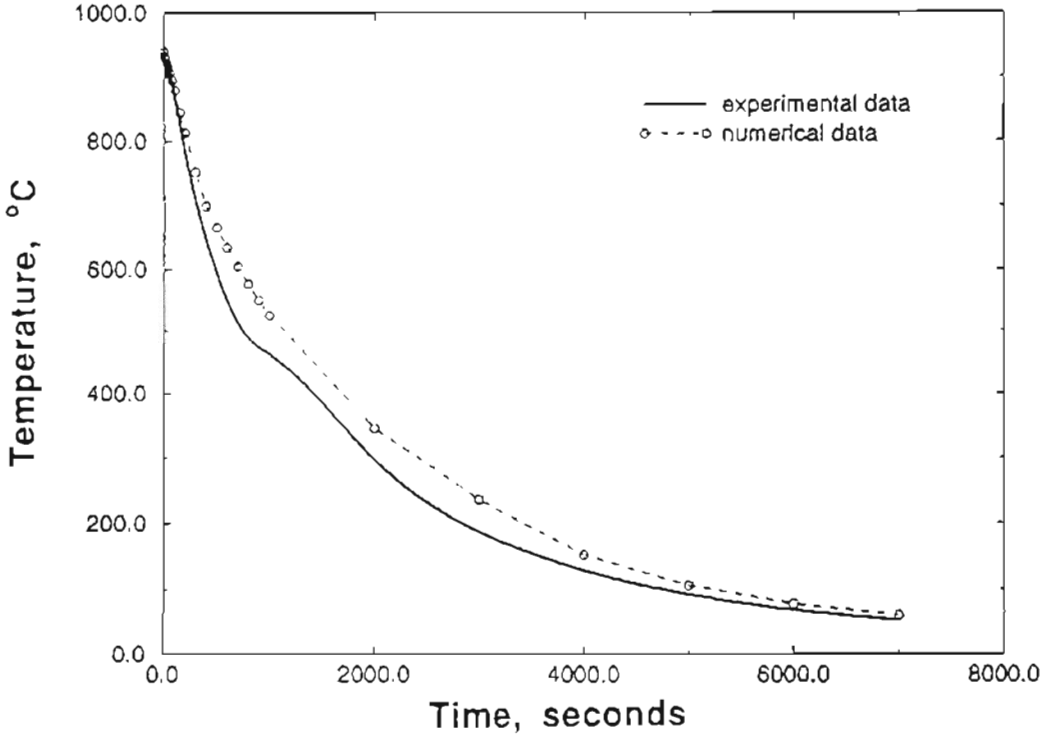

Figure 20. Comparison between measured and FEA calculated cooling characteristics at the center of the cavity section; modified temperature dependency of volumetric specific heat capacity; air cooled from 950°C.

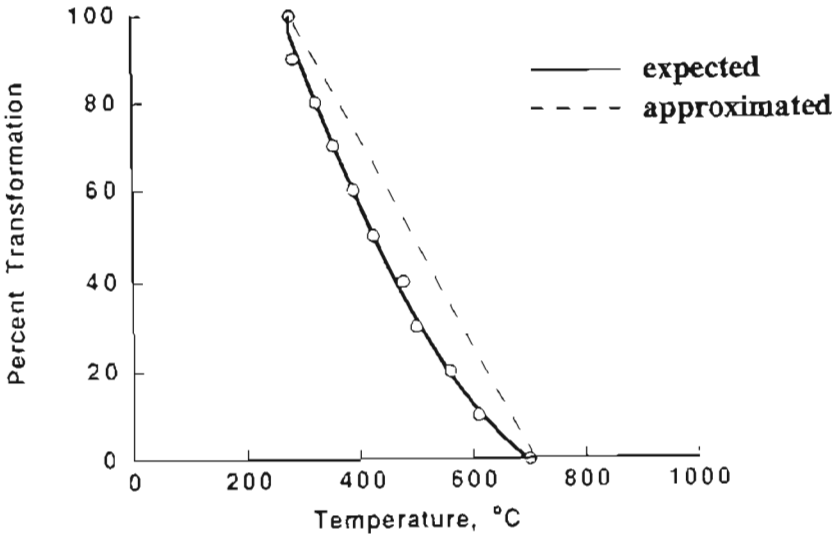

Figure 21. Expected and approximated transformation kinetics for the FE air cool model.

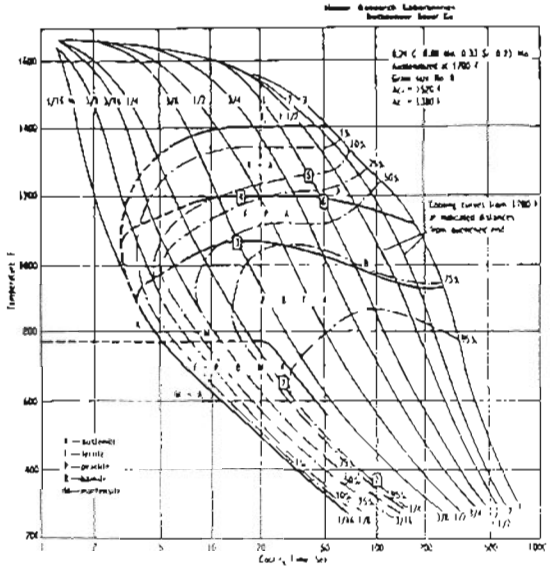

Figure 22. CCT diagram for AISI 4024 steel.

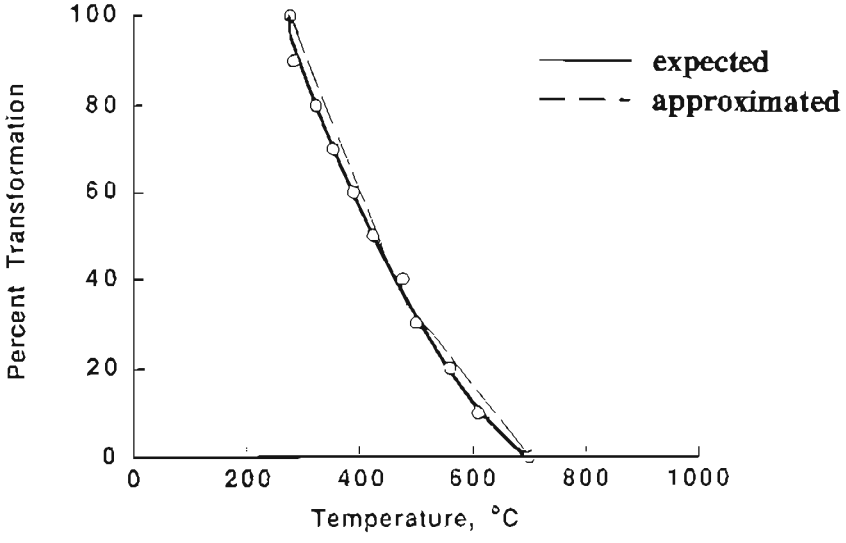

Figure 23. Expected and approximated transformation kinetics for the air cool FE model, based on kinetics observed in AISI 4024 steel.

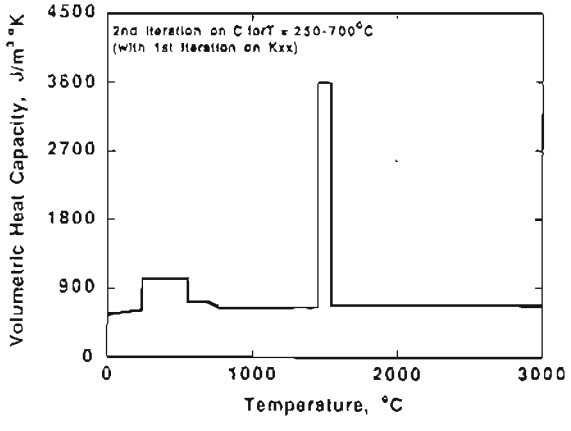

Figure 24. Second modification of the temperature dependency of the volumetric specific heat capacity used in the FEA.

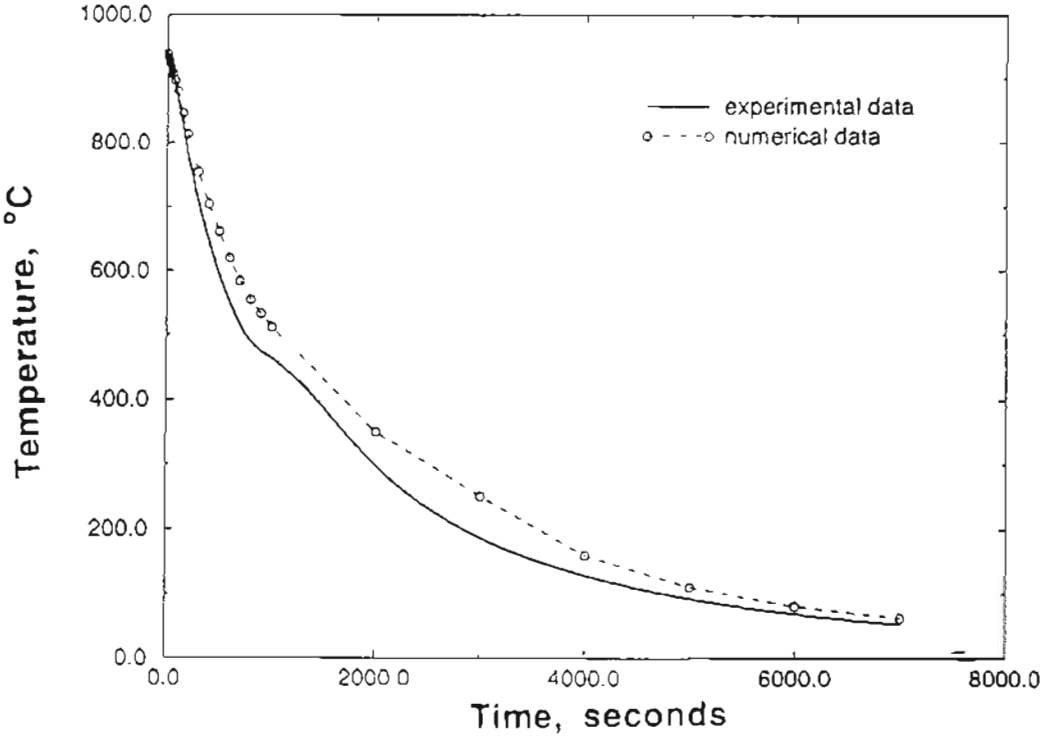

Figure 25. Comparison between measured and FEA calculated cooling characteristics at the center of the cavity section; second modification of temperature dependency of volumetric specific heat capacity; air cooled from 950°C.

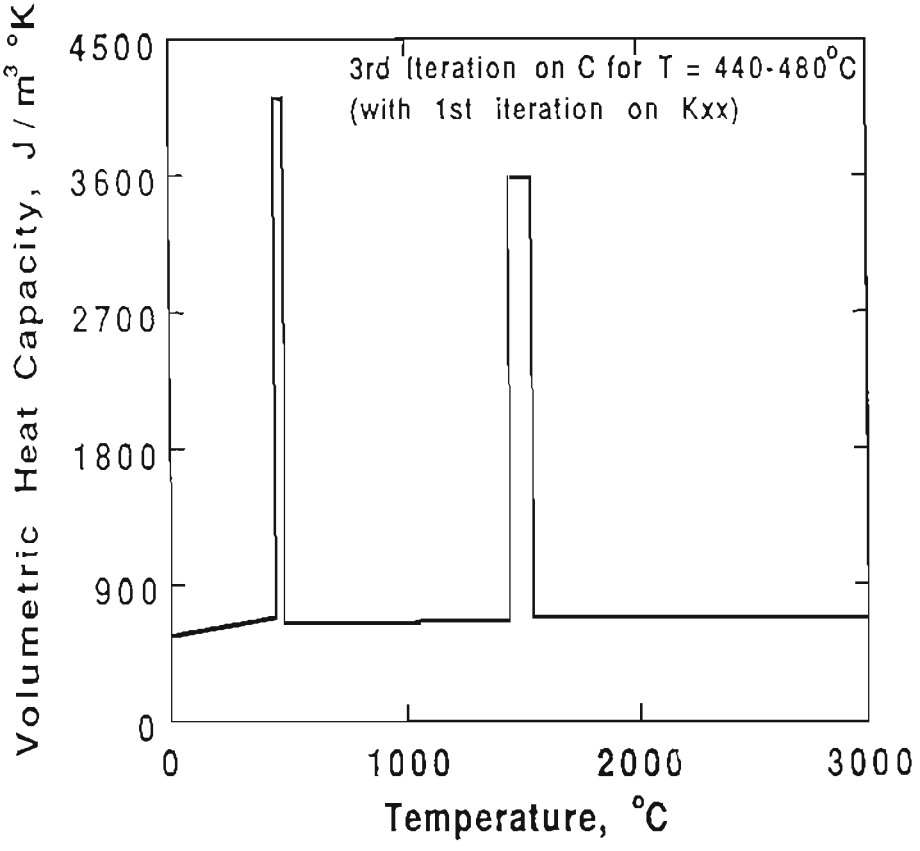

Figure 26. Third modification of the temperature dependency of the volumetric specific heat capacity used in the FEA.

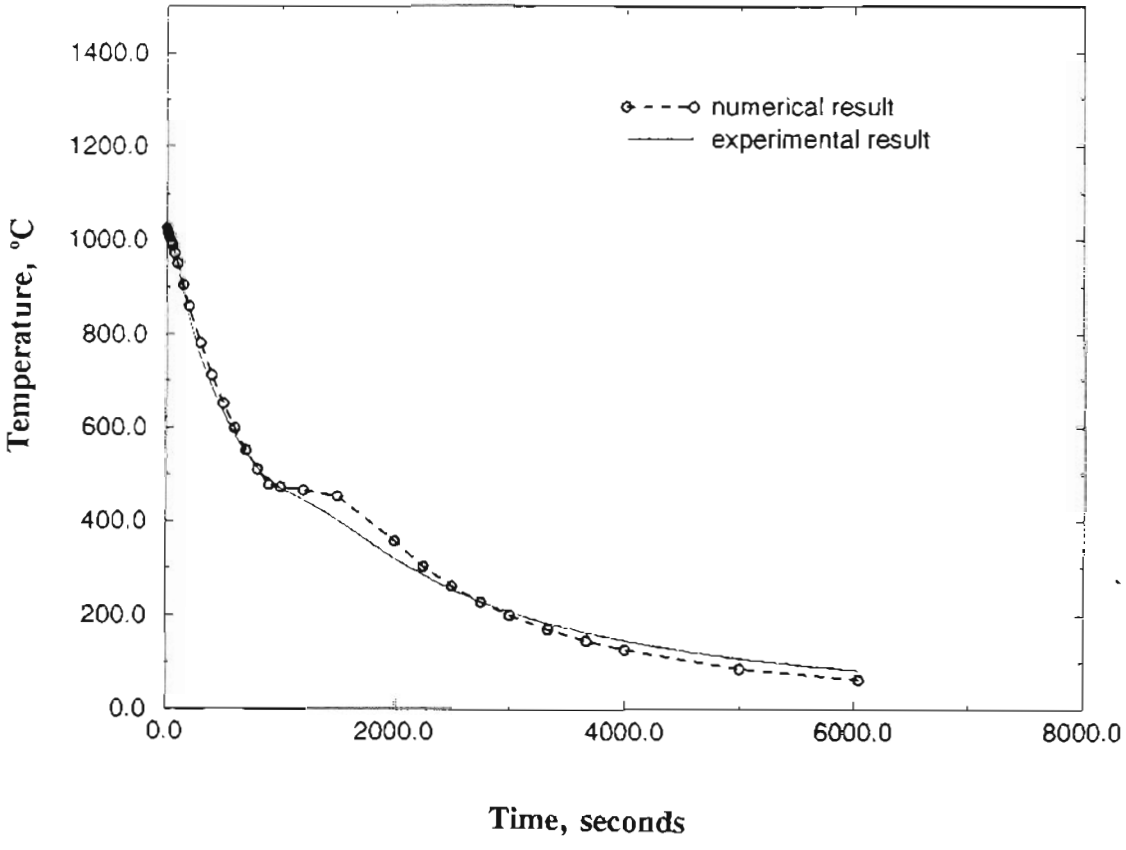

Figure 27. Comparison of measured and FEA calculated cooling characteristics at the center of the cavity section; third modification of temperature dependency of the volumetric specific heat capacity; air cooled from 1040°C.

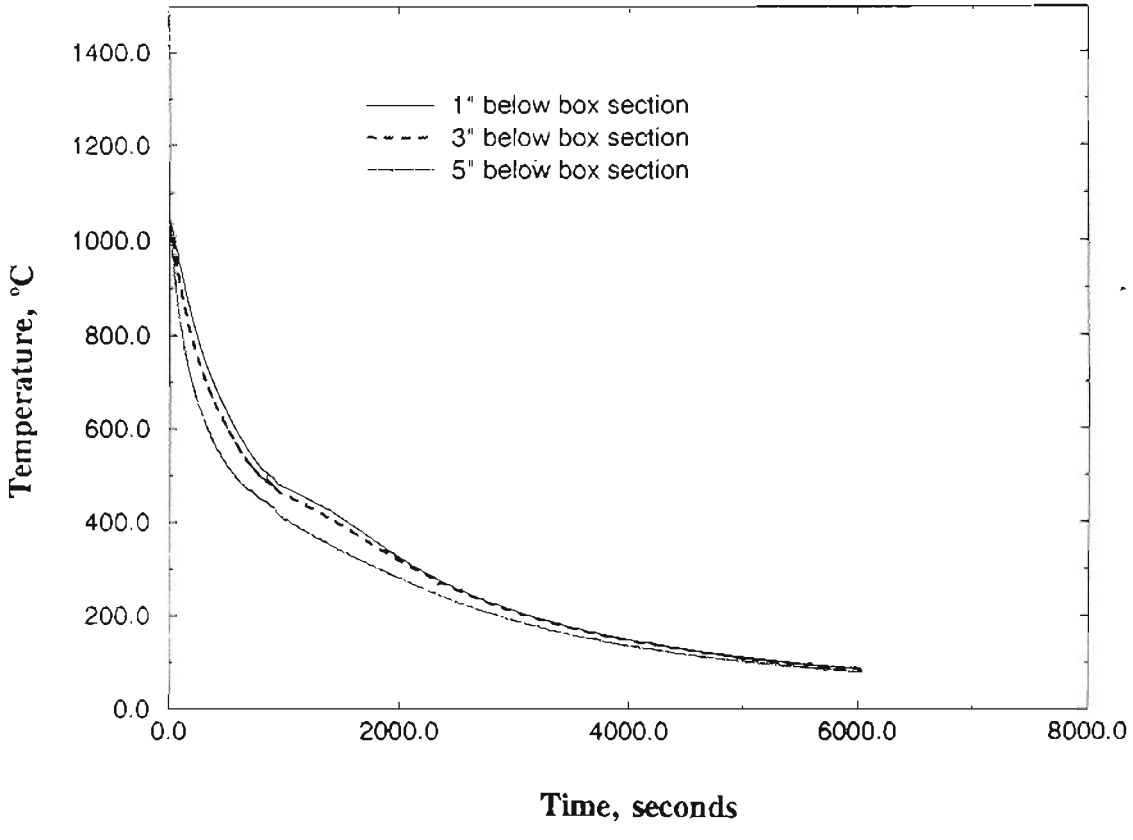

Figure 28. Measured cooling characteristics at locations 1" below, 3" below and 5" below the surface of the cavity section and along the axis of symmetry; air cooled from 1040°C.

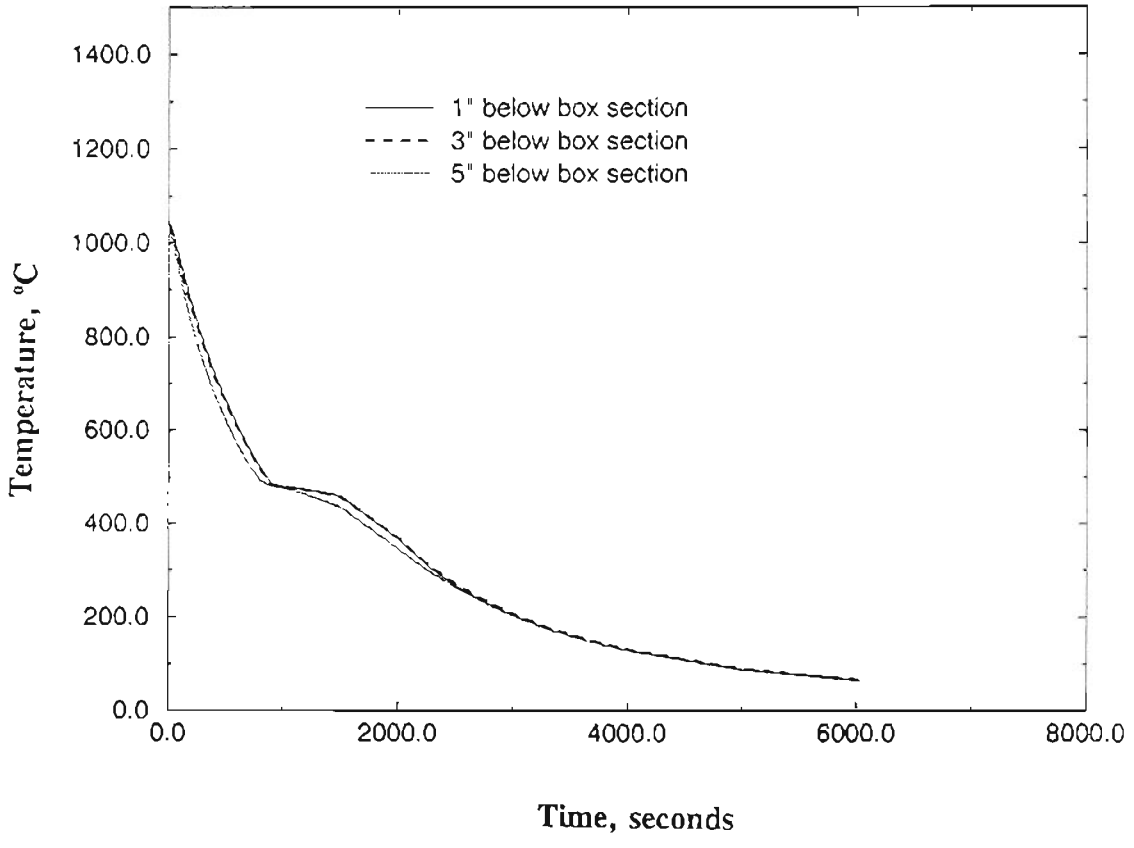

Figure 29. Calculated cooling characteristics at locations 1" below, 3" below and 5" below the surface of the cavity section and along the axis of symmetry; air cooled from 1040oC.

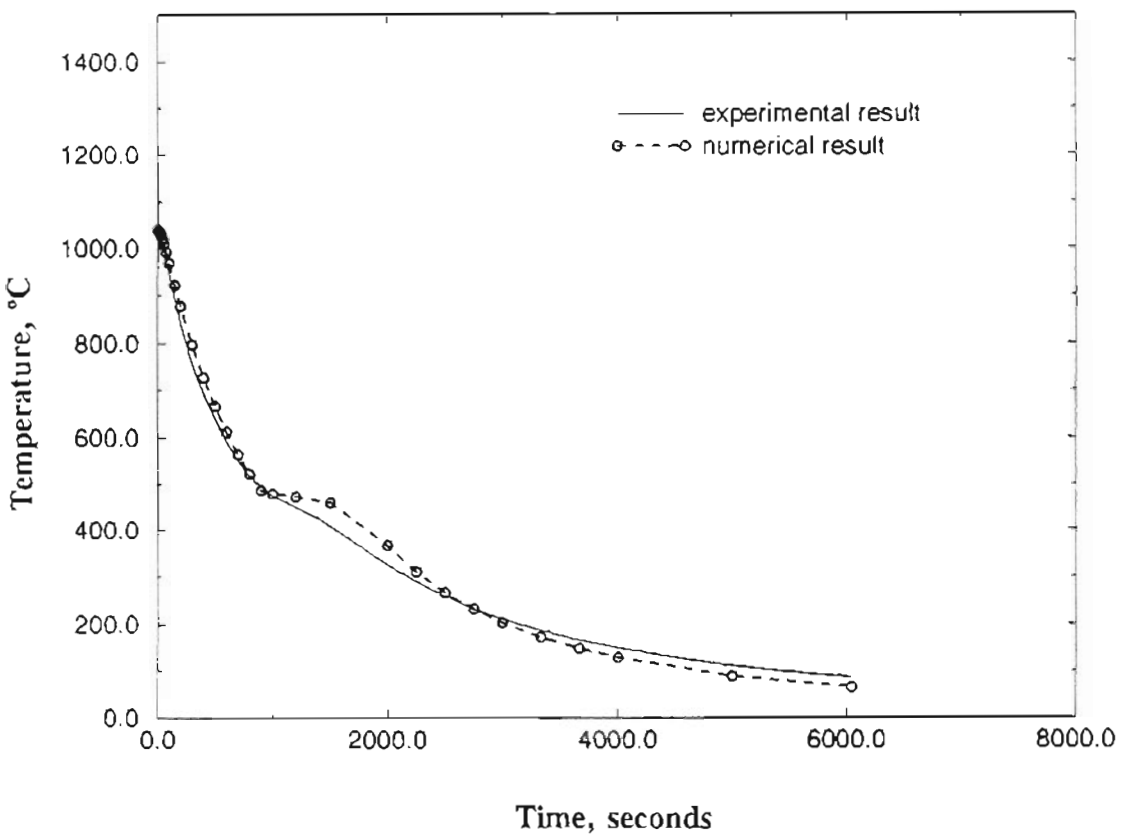

Figure 30. Comparison of measured and calculated cooling characteristics at the 1"-below location; air cooled from 1040°C.

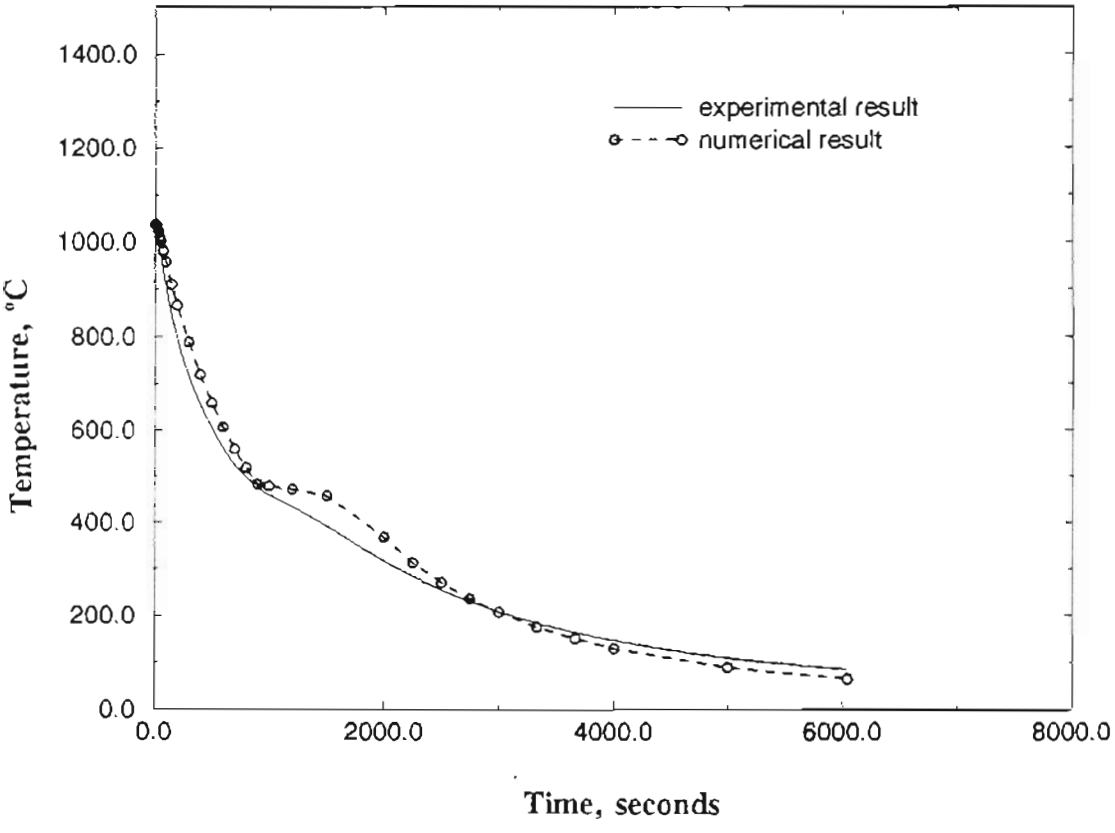

Figure 31. Comparison between measured and FEA calculated cooling characteristics at the 3"-below location; air cooled from 1040°C.

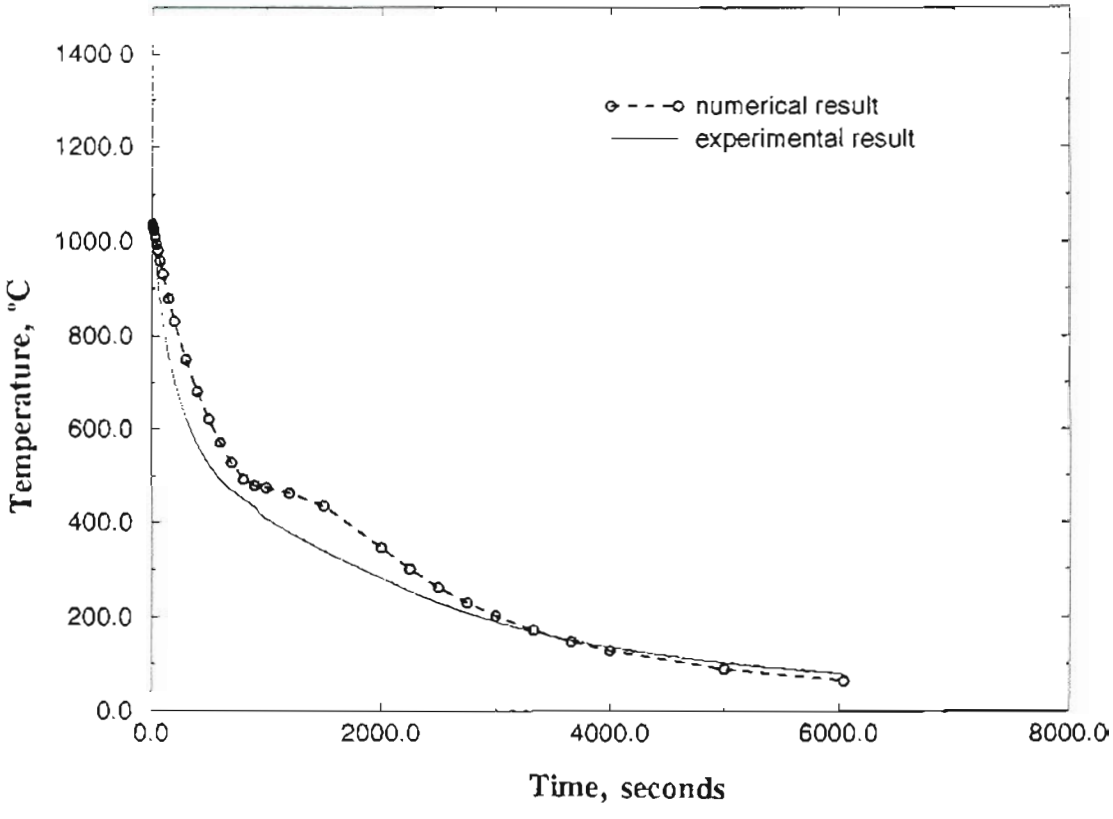

Figure 32. Comparison between measured and FEA calculated cooling characteristics at the 5"-below location; air cooled from 1040°C.

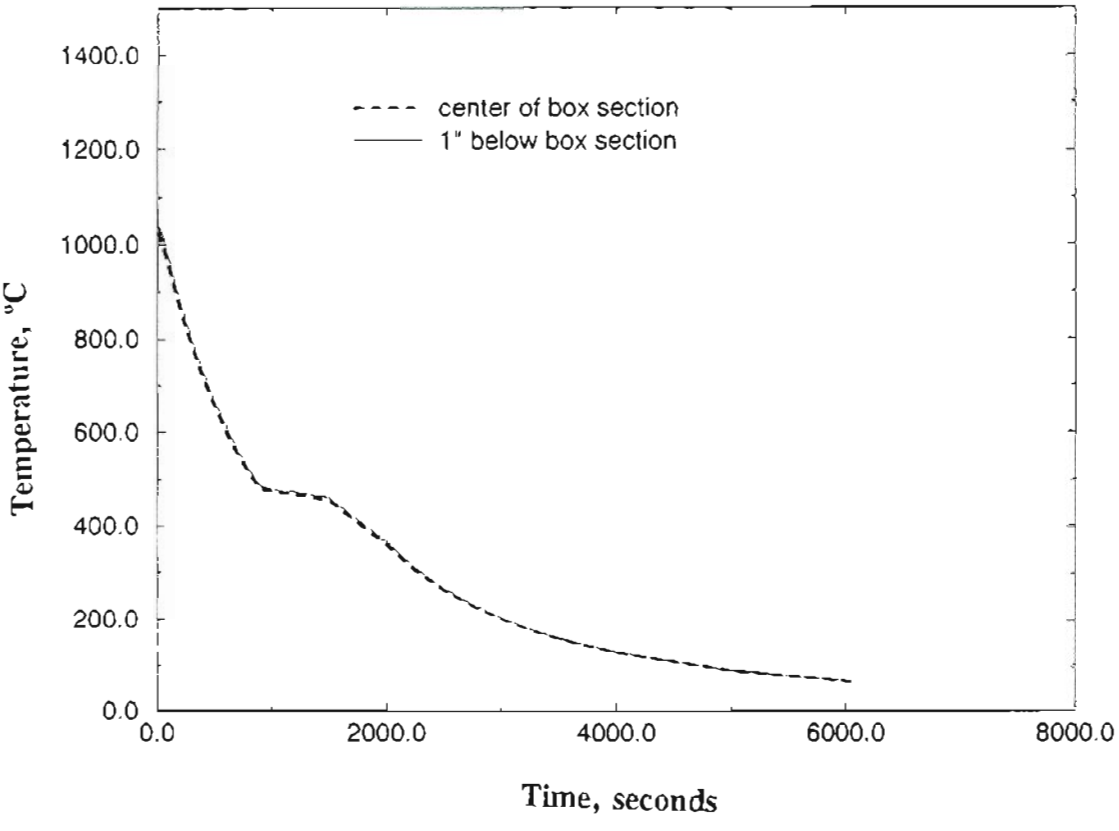

Figure 33. FEA calculated variation in cooling characteristics between center of the cavity section and 1"-below location; air cooled from 1040°C.

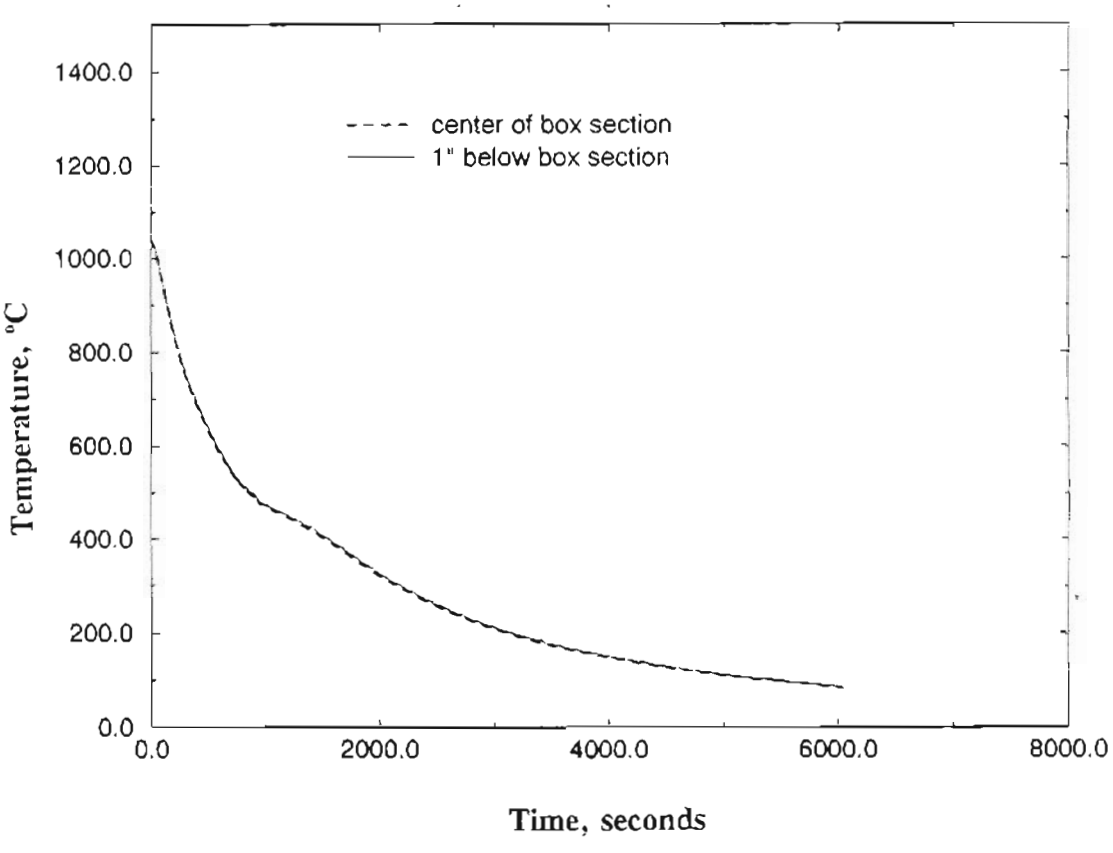

Figure 34. Measured variation in cooling characteristics between center of cavity section and 1"-below location; air cooled from 1040°C.

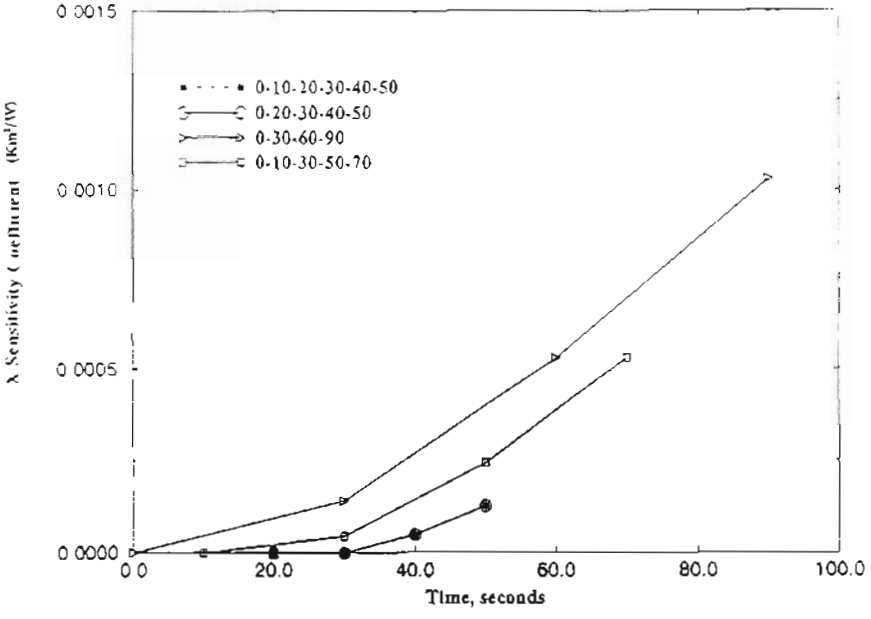

Figure 35. Temporal disretization effects.

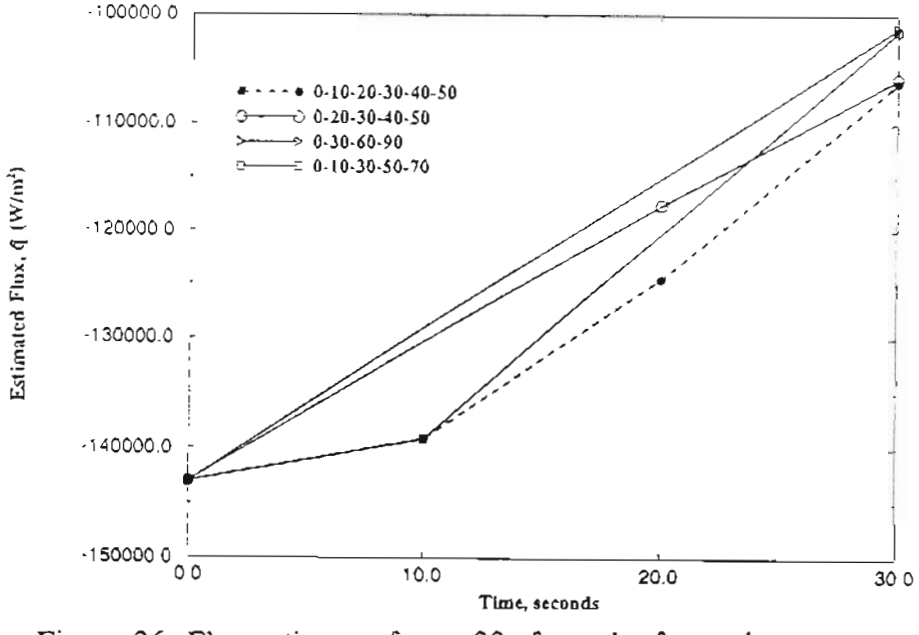

Figure 36. Flux estimates for t=30s from the four schemes.

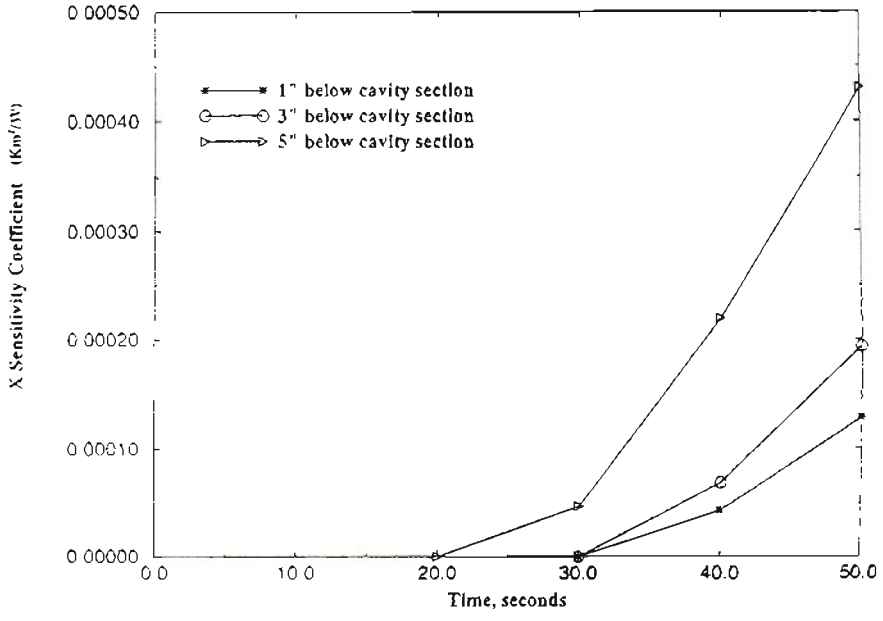

Figure 37. Sensor location effects for the 0-10-20-30-40-50 scheme

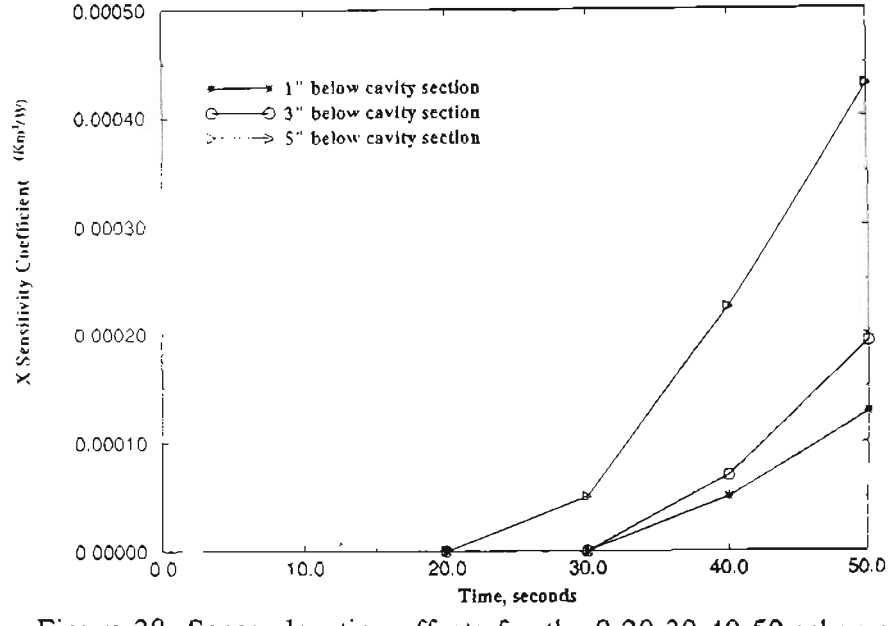

Figure 38. Sensor location effects for the 0-20-30-40-50 scheme.

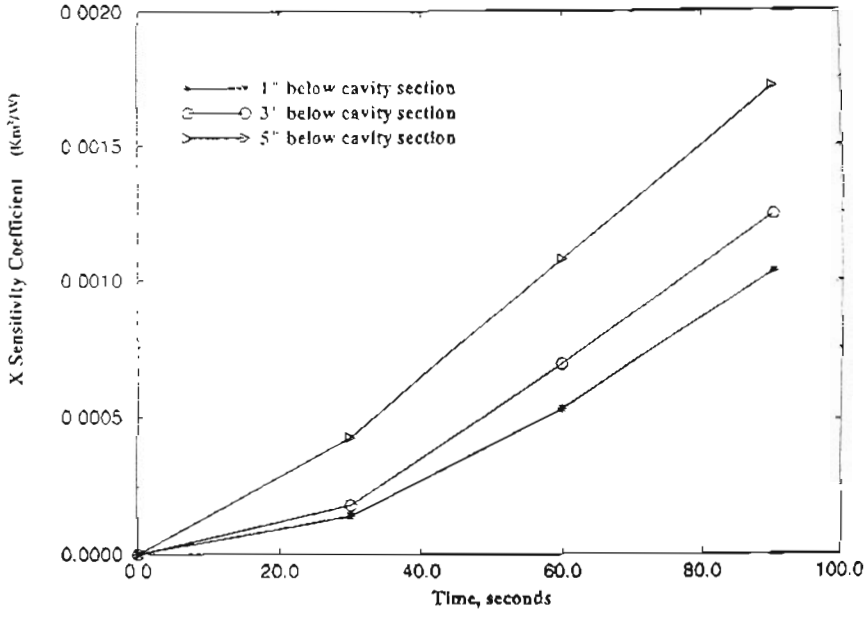

Figure 39. Sensor location effects for the 0-30-60-90 scheme.

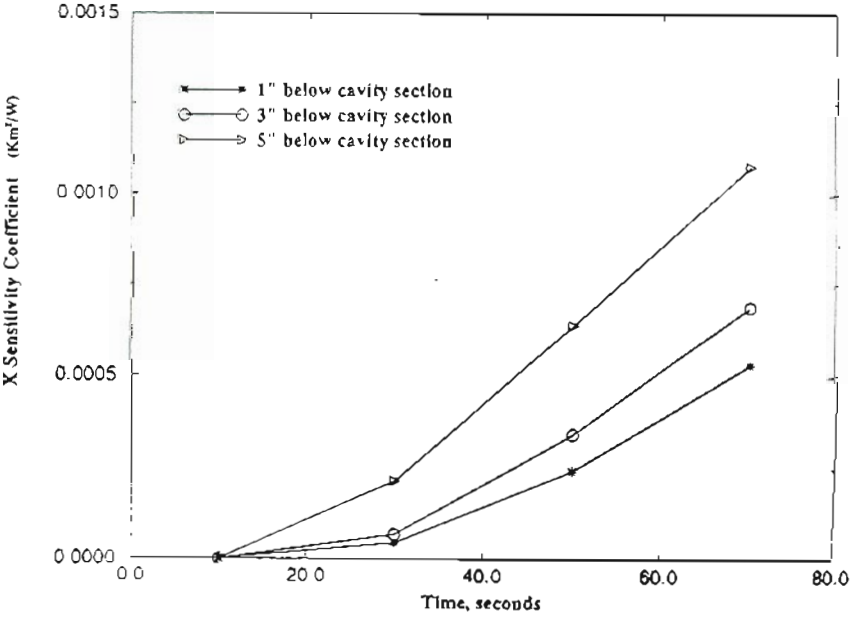

Figure 40. Sensor location effects for the 0-10-30-50-70 scheme.

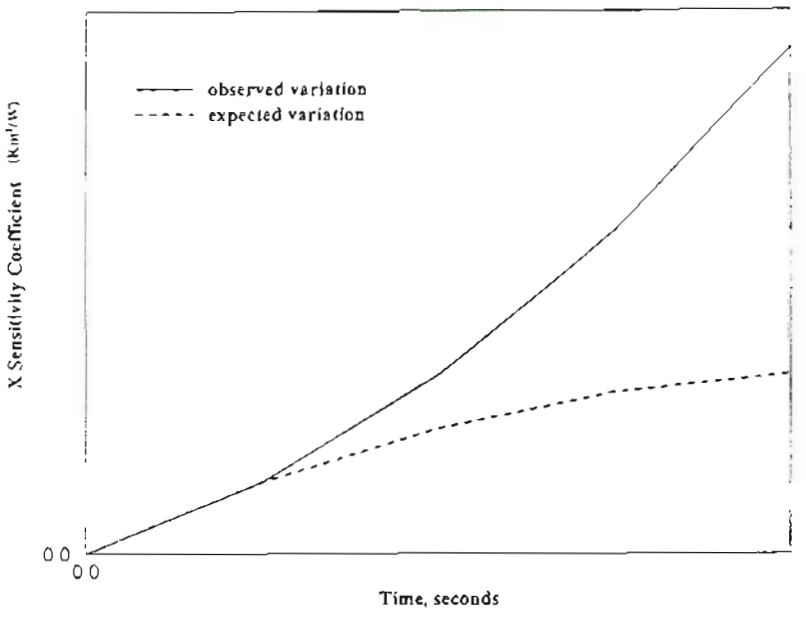

Figure 41. Observed and expected variation of sensitivity coefficient with cooling duration.

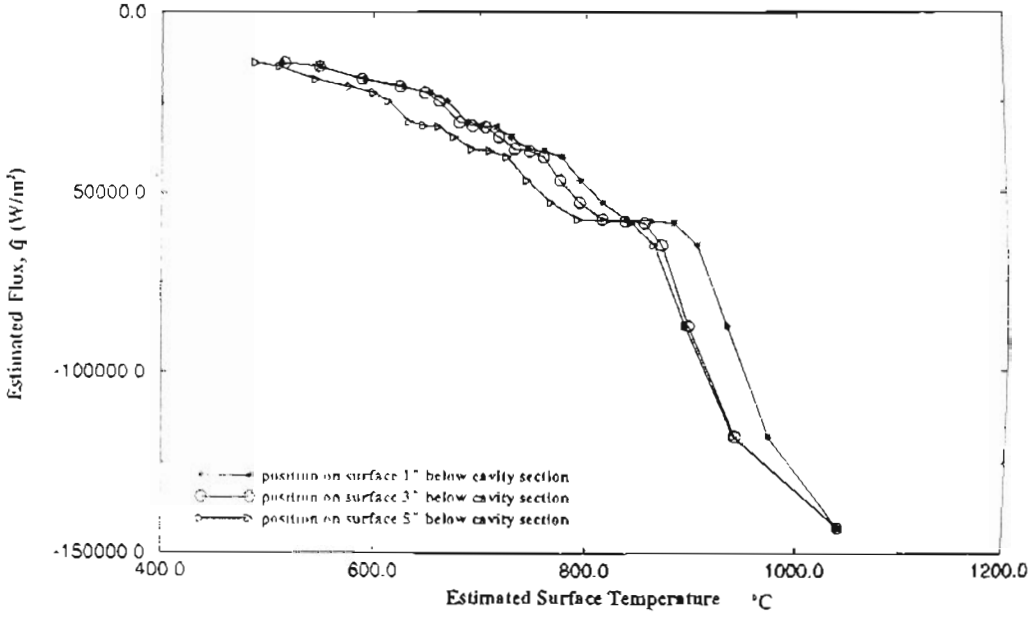

Figure 42. Estimated flux history.

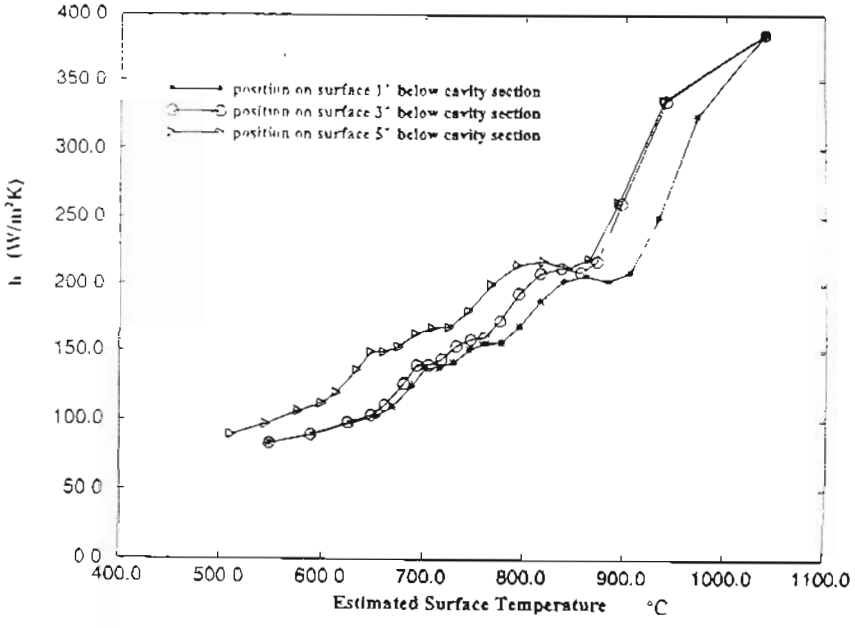

Figure 43. Estimated temperature dependency of the convective heat transfer coefficient for air.

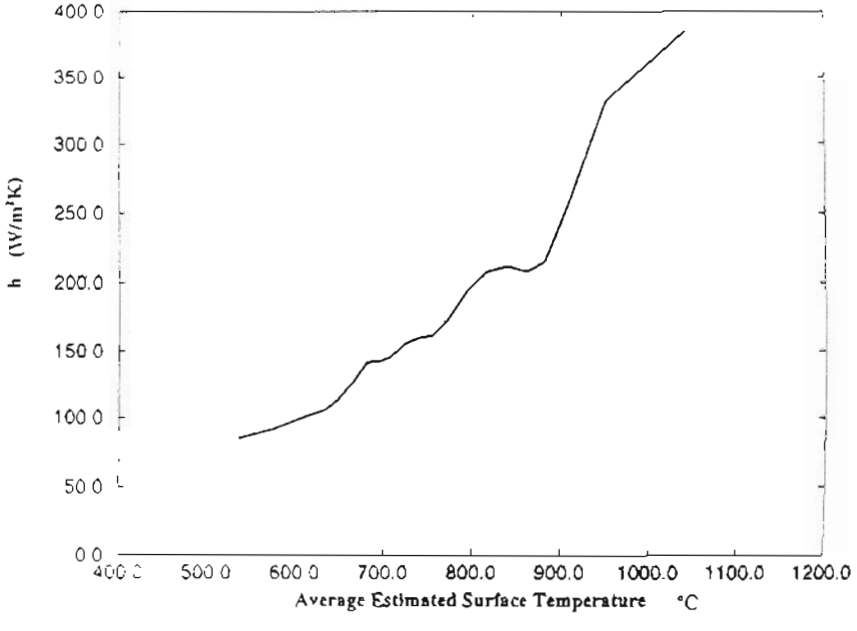

Figure 44. Estimated convective heat transfer coefficient for air as a function of average estimated surface temperature.

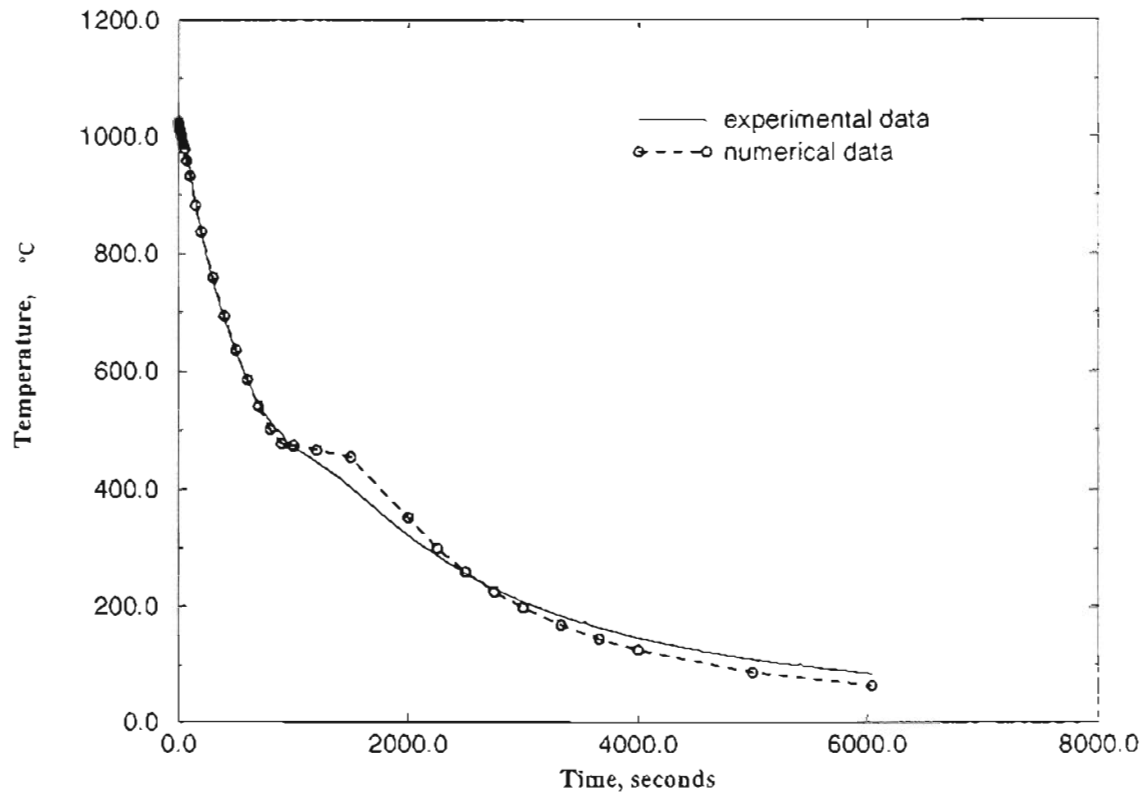

Figure 45. Comparison between measured and FEA calculated cooling characteristics at the center of the cavity section; temperature dependent convective heat transfer coefficient calculated using inverse method used in the FEA; air cooled from 1040°C.

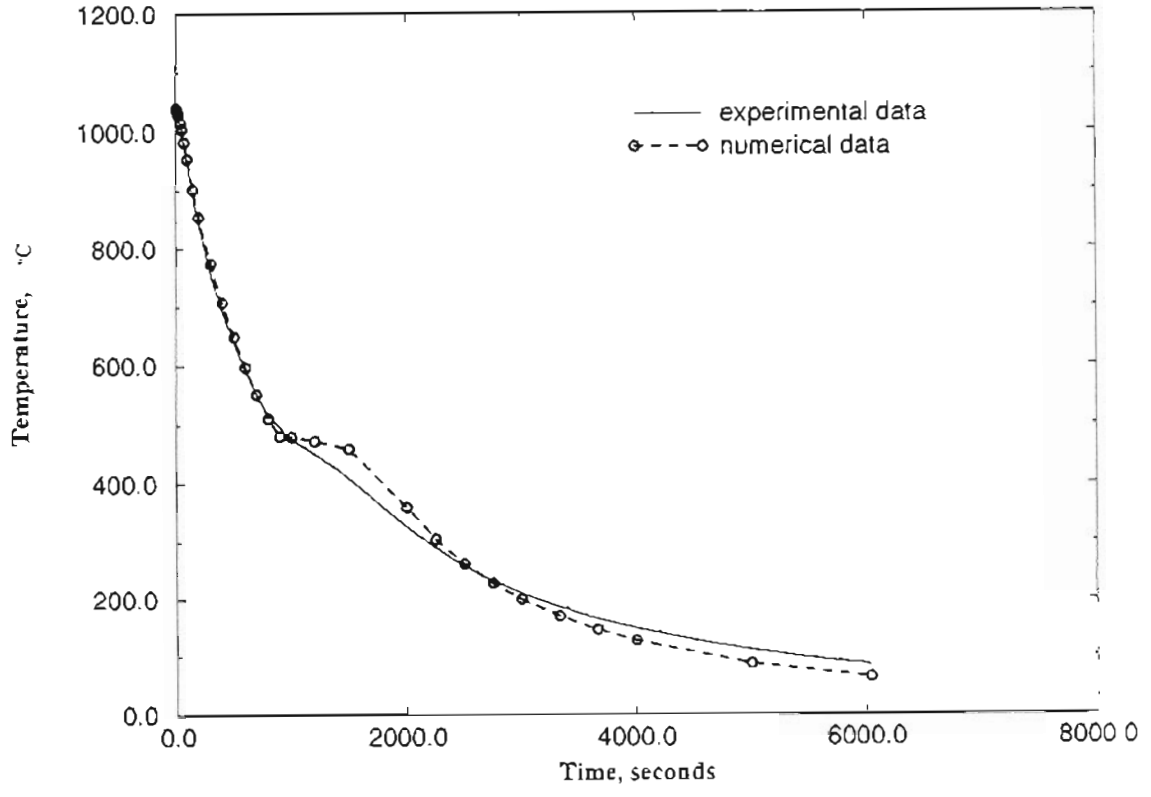

Figure 46. Comparison between measured and FEA calculated cooling characteristics at the 1"-below location; temperature dependent convective heat transfer coefficient calculated using inverse method used in the FEA; air cooled from 1040°C.

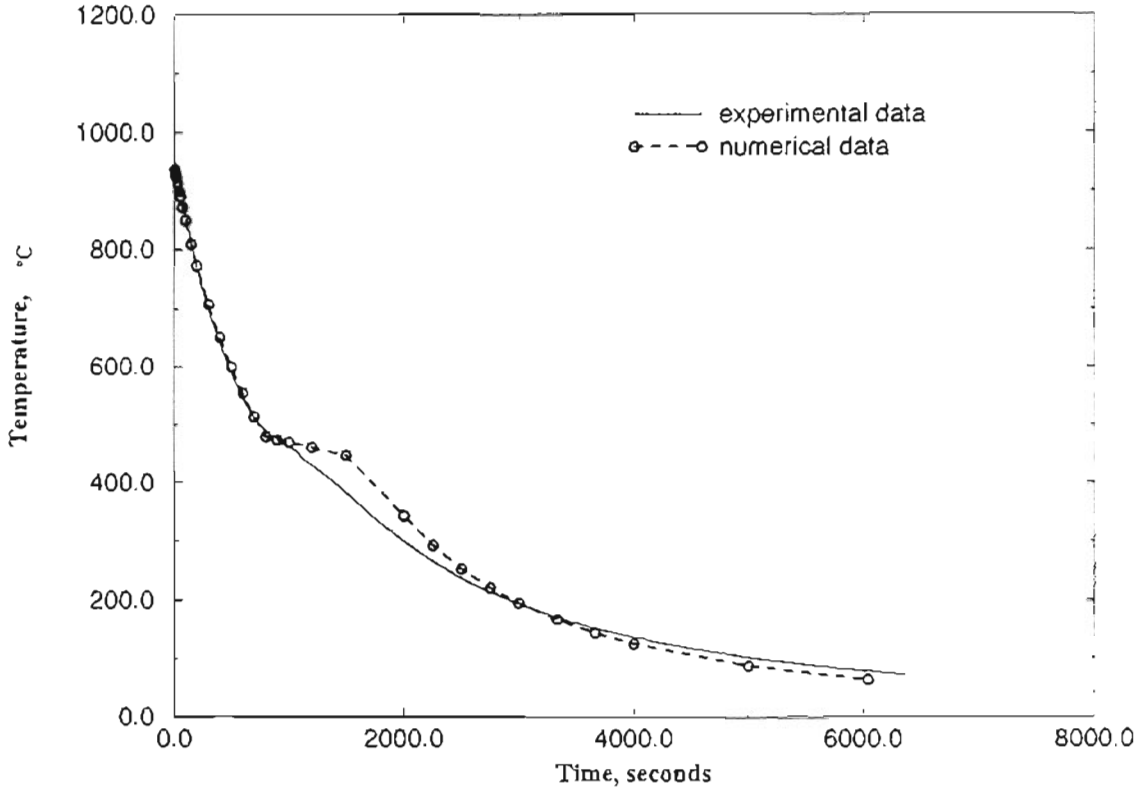

Figure 47. Comparison between measured and FEA calculated cooling characteristics at the 2"-below location; temperature dependent convective heat transfer coefficient calculated using inverse method used in the FEA; air cooled from 950°C.

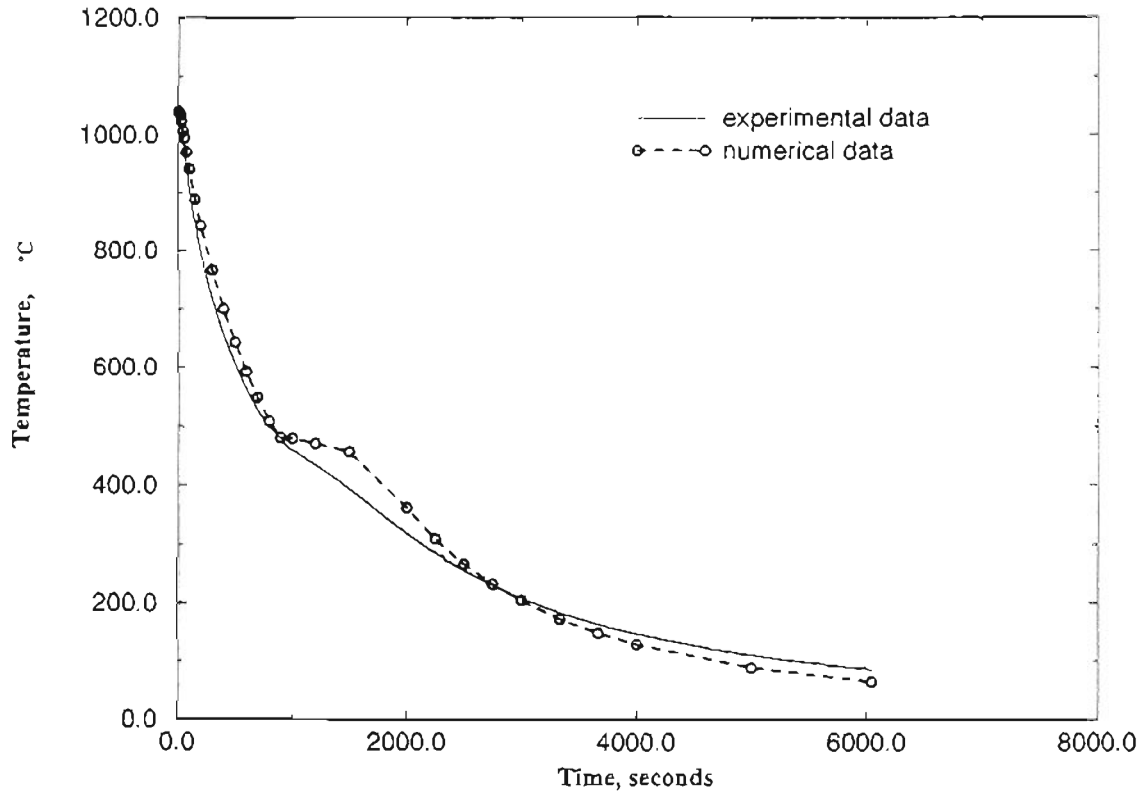

Figure 48. Comparison between measured and FEA calculated cooling characteristics at the 3"-below location; temperature dependent convective heat transfer coefficient calculated using inverse method used in the FEA; air cooled from 1040°C.

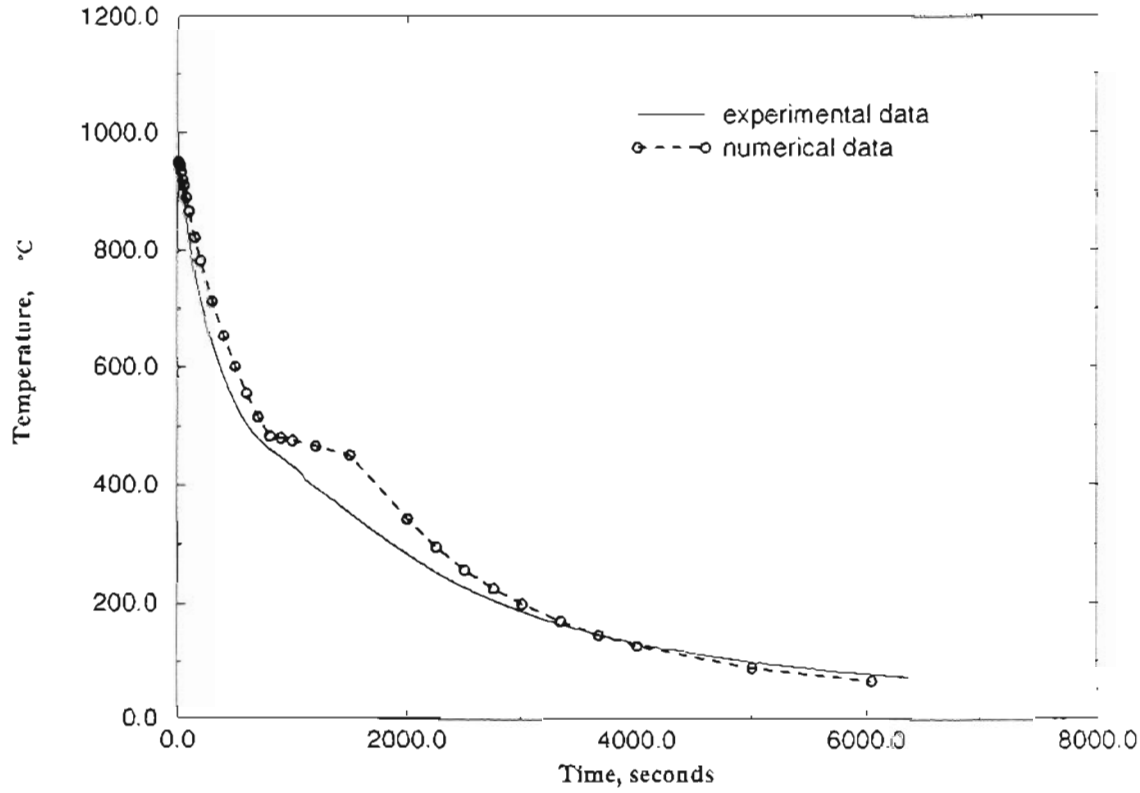

Figure 49. Comparison between measured and FEA calculated cooling characteristics at the 4"-below location; temperature dependent convective heat transfer coefficient calculated using inverse method used in the FEA; air cooled from 950°C.

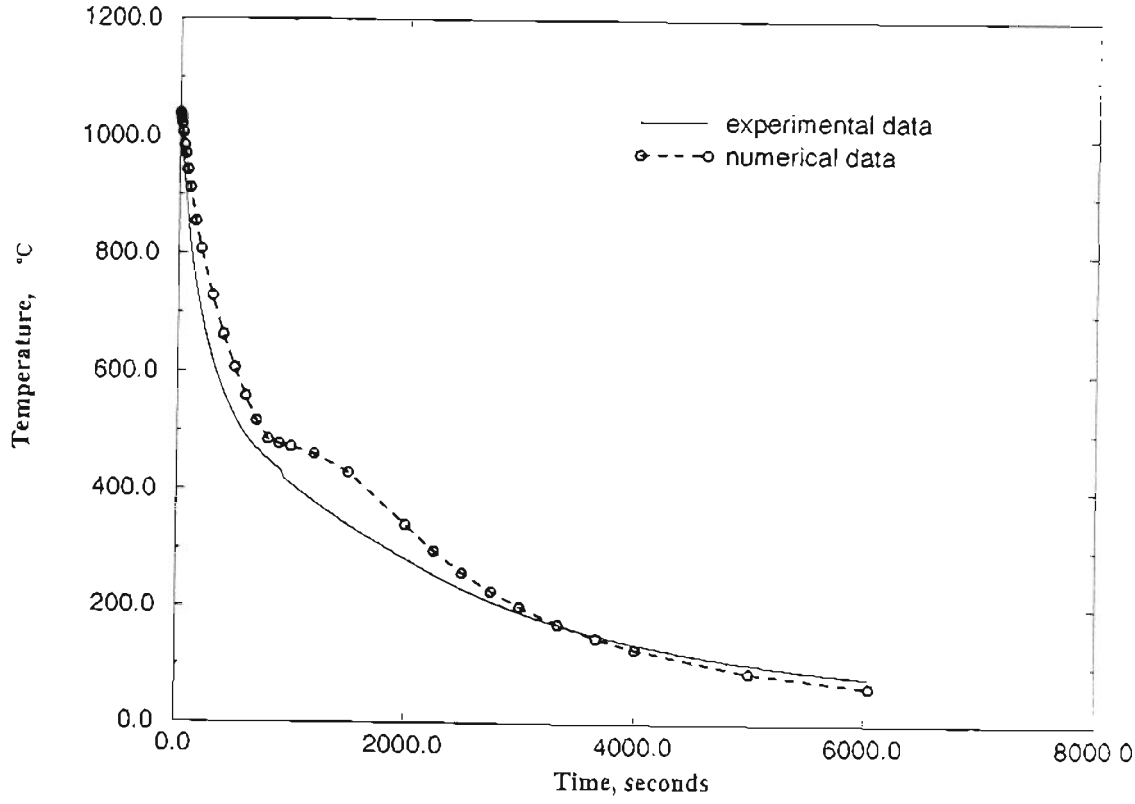

Figure 50. Comparison between measured and FEA calculated cooling characteristics at the 5"-below location; temperature dependent convective heat transfer coefficient calculated using inverse method used in the FEA; air cooled from 1040°C.

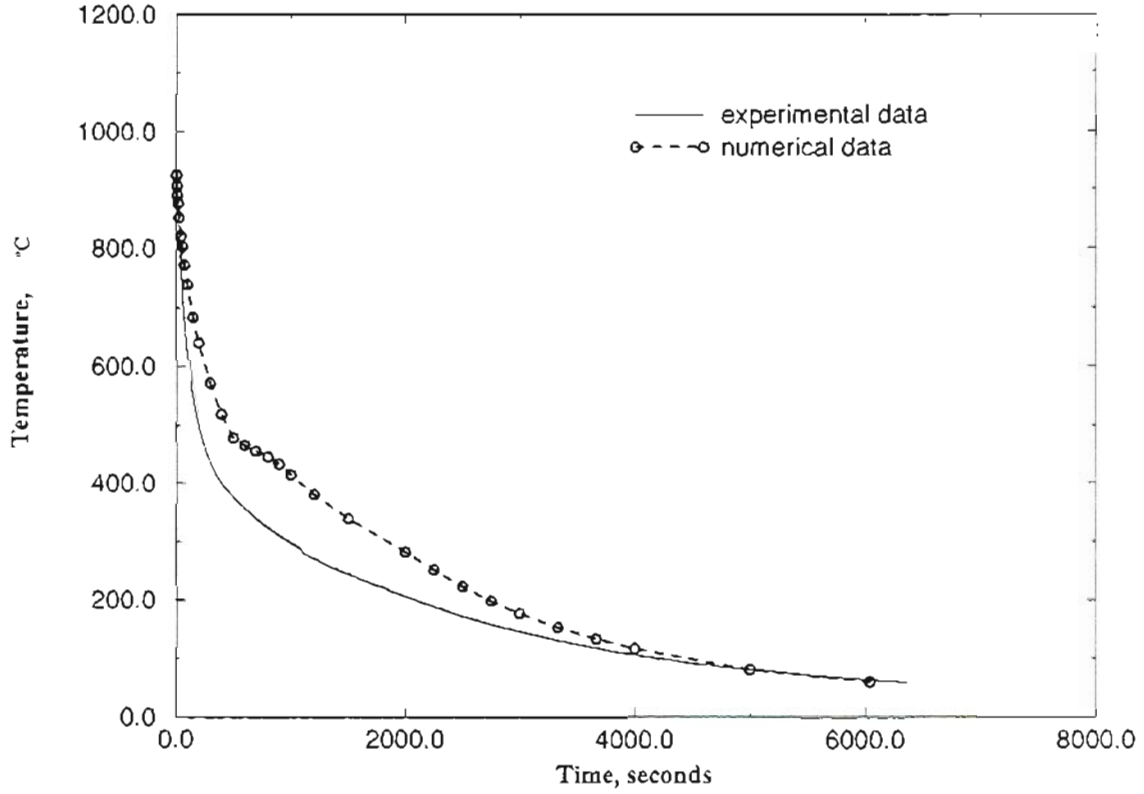

Figure 51. Comparison between measured and FEA calculated cooling characteristics at the tip of the specimen; temperature dependent convective heat transfer coefficient calculated using inverse method used in the FEA; air cooled from 950°C.

REFERENCES

1. C.E.Henwood, "An Analytical Model for Computing Weld Microstructures", Carleton University, Ottawa, Canada, M.Eng. Thesis, 1987.

2. J.C.Ion, K.E.Easterling, M.F.Ashby, "A Second Report on Diagrams of Microstructure and Hardness for Heat-Affected Zones in Welds", Acta Metallurgica, 1984, Vol.32, No.11

3. J.S.Kirkaldy, D.Venugopalan, "Prediction of Microstructure and Hardenability in Low Alloy Steels", Phase Transformations in Ferrous Alloys, Proceedings of the International Conference, Oct.4-6, 1983.

4. L.Beresford, "Finite Element Analysis of Three Dimensional Transient Heat Flow in Solids", Carleton University, Ottawa, Canada, M.Eng. Thesis, 1983.

5. J.Goldak, B.Patel, M.Bibby, J.Moore, "Computational Weld Mechanics", invited opening paper for AGARD Workshop- Structures and Materials, 61st Panel Meeting, Oberammergau, Germany, Sept. 8-13, 1989.

6. T.Inoue, D-Y.Ju, K.Arimoto, "Metallo-Thermo-Mechanical Simulation of Quenching Process- Theory and Implementation of Computer Code "HEARTS" ", Proceedings of the First International Conference on Quenching and Control of Distortion, Chicago, Illinois, USA, Sept. 22-25, 1992.

7. J.Bodin, S.Segerberg, "Benchmark Testing of Computer Programs for Determination

of Hardening Performance", Swedish Institute of Production Engineering Research, Goteborg, Sweden, presented at Proceedings of the First International Conference on Quenching and Control of Distortion; Chicago, Illinois, USA, Sept. 22-25, 1992.

8. B.Hernandez- Morales, J.K.Brimacombe, E.B.Hawbolt, S.M.Gupta, "Determination of Quench Heat-Transfer Coefficients Using Inverse Techniques", Proceedings of the First International Conference on Quenching and Control of Distortion, Chicago, Illinois, USA, Sept. 22-25, 1992.

9. J.V.Beck, A.M.Osman, "Analysis of Quenching and Heat Treating Processes Using Inverse Heat Transfer Method", Michigan State University, East Lansing, Michigan, presented at Proceedings of the First International Conference on Quenching and Control of Distortion, Chicago, Illinois, USA, Sept. 22-25, 1992.

10. S.Segerberg, J.Bodin, "Variation in the Heat Transfer Coefficient Around Components of Different Shapes During Quenching", Swedish Institute of Production Engineering Research, Goteborg, Sweden, presented at Proceeding of the First International Conference on Quenching and Control of Distortion, Chicago, Illinois, USA, Sept. 22-25, 1992.

11. B.Buchmayr, J.S.Kirkaldy, "A Fundamental Based Microstructure Model for the Optimization of Heat Treatment Processes", Proceeding of the First International Conference on Quenching and Control of Distortion, Chicago, Illinois, USA, Sept. 22-25, 1992.

12. J.V.Beck, B.Blackwell, C.R.St.Clair, Jr., "Inverse Heat Conduction : Ill Posed Problems", Wiley-Interscience, New York, 1985.

APPENDIX A

The fineness of a finite element mesh is generally limited to a finite number of degrees of freedom in commercial codes. This limitation is felt more acutely if coupled analyses, such as thermal/stress analyses, are to be performed, since the number of degrees of freedom are now higher. Specifically, the number of degrees of freedom and complexity of computations for structural analysis are higher than for thermal analysis. The original finite element mesh, shown in figure 5, was designed to satisfy the constraints of a coupled analysis. However, since the emphasis of this study was heat transfer analysis, a finer, more uniform mesh, shown in figure A1, was used.

The contribution of radiation in the estimation of the outgoing flux from the cooling specimen is incorporated in the inverse heat transfer method used in this work. Conceptually, a flux is calculated such that a least squares error accumulated over several sensors in minimized. This methodology of flux estimation does not distinguish between the different modes of heat energy dissipation i.e; convection and/or radiation.

Finally, the inverse method may possibly be used to estimate the latent heat released when solid state phase transformations occur. This estimate could then be approximated to determine the temperature dependency of the volumetric heat capacity over this temperature range. The actual procedure would involve the application of the inverse method twice. First, the transient temperature history from an interior location of a lumped geometry of the desired steel chemistry has to be obtained, as the body cools. With this data, the inverse method can be used to estimate the flux history in the temperature range over which the phase transformations occur. Next, the experimental cooling curve may be approximated to represent a transformation"less" situation, for which, the inverse method can be applied once again to estimate the flux history without the contribution due to phase transformations. The difference between the two estimates

will provide an initial approximation of the energy release rates in the relevant temperature range.

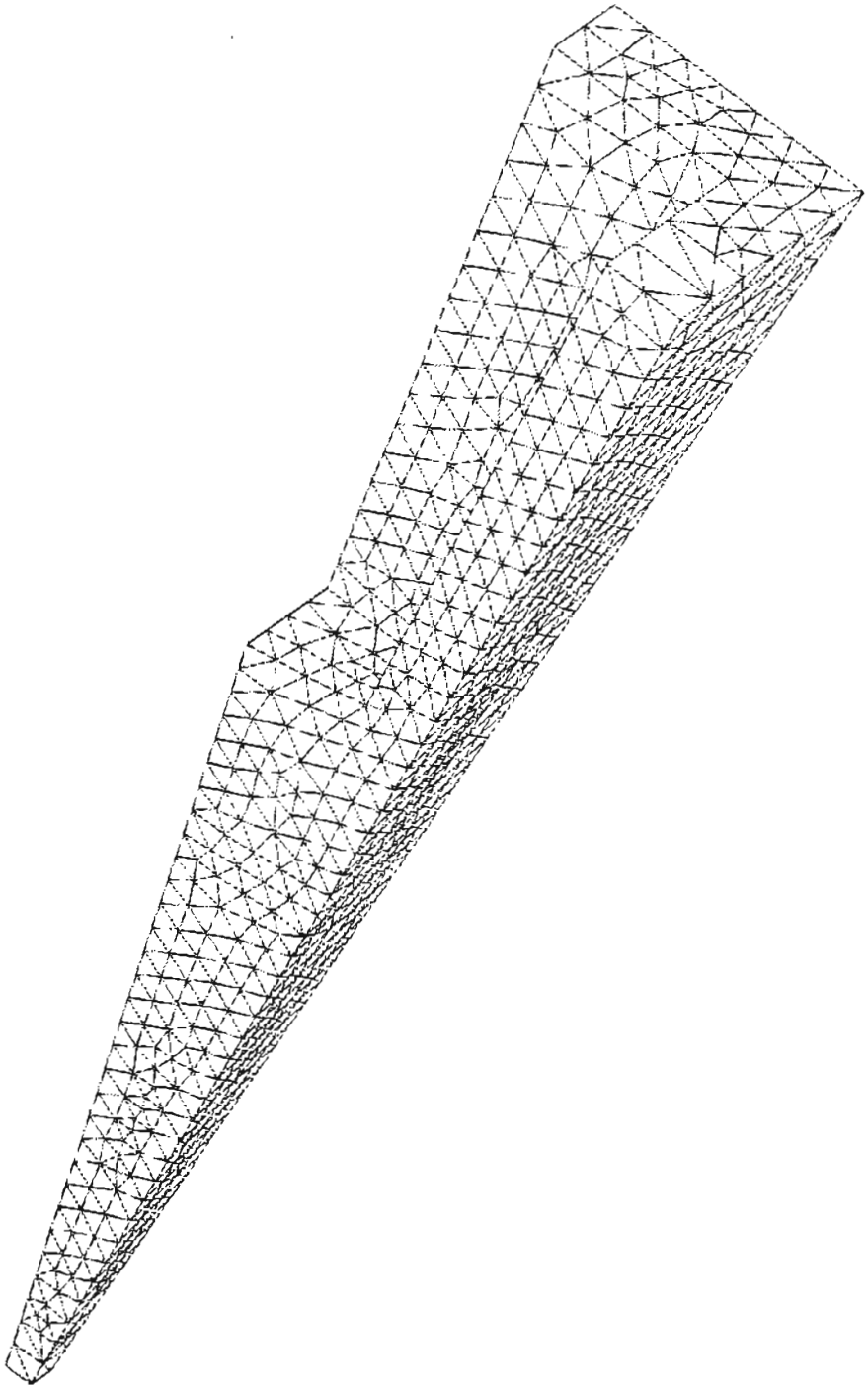

Figure A1. Finite element mesh of the quarter symmetry model after refinement

BIOGRAPHICAL SKETCH

The author was born on the 24th of April, 1968 in Vellore, India. He was awarded a B.Tech. in Metallurgical Engineering from the Indian Institute of Technology, Madras in June, 1991. That same year, he joined the Department of Materials Science and Engineering at the Oregon Graduate Institute of Science and Technology. Upon completion of his work towards a Master's degree, he proceeds to pursue a doctorate degree at Vanderbilt University. His specific area of interest is in the applications of numerical methods in Materials Science. He has been invited to present some of the results from this work at a heat transfer modeling conference in Florida this winter.